Depart of Chemistry

Redox reactions in deep eutectic solvents: characterisation and application

David Lloyd

A!

DOCTORAL DISSERTATIONS

Aalto University publication series
DOCTORAL DISSERTATIONS 174/2013

Redox reactions in deep eutectic solvents: characterisation and application

David Lloyd

A doctoral dissertation completed for the degree of Doctor of Science (Technology) to be defended, with the permission of the Aalto University School of Chemical Technology, at a public examination held at the lecture hall KE2 (Komppa Auditorium) at the Aalto University School of Chemical Technology (Espoo, Finland) on December 5th 2013 at noon.

Aalto University
School of Chemical Technology
Department of Chemistry
Laboratory for Physical Chemistry and Electrochemistry

Supervising professor
Kyösti Kontturi

Thesis advisor
Lasse Murtomäki

Preliminary examiners
Len Berlouis, University of Strathclyde, United Kingdom
Salvadore Mafé,University of Valencia, Spain

Opponents
Professor Andrew Abbott, University of Leicester, United Kingdom

Aalto University publication series
DOCTORAL DISSERTATIONS 174/2013

ISBN 978-952-60-5403-2
ISBN 978-952-60-5404-9 (pdf)
ISSN-L 1799-4934
ISSN 1799-4934 (printed)
ISSN 1799-4942 (pdf)
http://urn.fi/URN:ISBN:978-952-60-5404-9

Unigrafia Oy
Helsinki 2013

Finland

441 697
Printed matter

Author
David Lloyd

Name of the doctoral dissertation
Redox reactions in deep eutectic solvents: characterisation and application

Publisher School of Chemical Technology

Unit Department of Chemistry

Series Aalto University publication series DOCTORAL DISSERTATIONS 174/2013

Field of research Electrochemistry

Manuscript submitted 30 September 2013 **Date of the defence** 5 December 2013

Permission to publish granted (date) 8 October 2013 **Language** English

☐ **Monograph** ☒ **Article dissertation (summary + original articles)**

Abstract

Ionic liquids are a field of intense chemical research activity due to their potential to facilitate a wide range of chemical innovations. Due to the cost of ionic liquids alternative materials which exhibit similar properties, but are less expensive, are also the subject of interest and deep eutectic solvents are a prime example.

Deep eutectic solvents are commonly based on quaternary ammonium chloride salts and therefore allow the ready dissolution of a range of metal chloride salts to form transition metal complexes. The electrolytes formed in this manner have been proposed as the basis for a range of novel processes to electrodeposit metals.

This thesis presents the first application of a range of electroanalytical techniques to quantitatively characterize the properties of electrochemical reactions involving copper and iron chloro complexes in deep eutectic solvents. The methods used are based on cyclic voltammetry, electrochemical impedance spectroscopy and potential steps. Methods based on both static and hydrodynamic electrodes are considered. The reactions are found to be equally kinetically facile as in aqueous solvents, however the relatively viscous nature of the solvent is reflected in the transport properties of the complexes formed. The successful application of these techniques required the development of a suitably responsive reference electrode system. A system employing a quasireference electrode and reference probe in parallel was found to provide both a well-defined reference potential and suitably low impedance.

The application of deep eutectic solvents in redox flow batteries is also reported for the first time and shown to allow the simple application of transition metal chlorocomplexes. However, the inferior transport properties of the electrolyte is shown to currently be a limiting factor within the temperature range studied. This requires the application of current densities at least an order of magnitude lower than those typically used in redox flow batteries. Application of deep eutectic solvents as the media for redox flow batteries required the development of a novel separator material based on jellification of the electrolyte using polyethylene glycol, this material was found to possess comparable conductivity to the pure electrolyte.

Keywords Ionic liquids, Deep Eutectic Solvents, Transition metal chloro complexes, Electrochemistry, Electrochemical Impedance Spectroscopy, Rotating Disc Electrode, Redox Flow Battery

ISBN (printed) 978-952-60-5403-2 **ISBN (pdf)** 978-952-60-5404-9

ISSN-L 1799-4934 **ISSN (printed)** 1799-4934 **ISSN (pdf)** 1799-4942

Location of publisher Helsinki **Location of printing** Helsinki **Year** 2013

Pages 135 **urn** http://urn.fi/URN:ISBN:978-952-60-5404-9

Preface

Firstly, I would like to thank my supervisor, Kyösti Kontturi, for the freedom he has given to me during the last five years. It is a great credit to him, and Anna-Kaisa Kontturi, that they have created a laboratory where good science can flourish without any compromises being made to the work-life balance. The level of confidence they have in the competence and honesty of the people who work for them is inspiring, humbling and typically Finnish.

Secondly, I would like to thank my colleague and sparring partner, Tuomas Vainikka, for the enormous assistance he has given me during this work, both of a practical and theoretical nature. Watching Tuomas work has been a lesson in determination, workmanship and Finnish 'sisu'.

Thirdly, my thanks also go to Pekka Peljo and Annukka Santasalo-Aarnio for providing the original inspiration to explore the fertile and fascinating interface between the realms of electroanalytical measurements and the development of actual energy conversion devices.

Also deserving of special gratitude are Elisabet Ahlberg for kickstarting my first publication, Lasse Murtomäki for teaching me the little I have managed to learn of impedance spectroscopy, Sönke Schmachtel for introducing me to Matlab, Ben Wilson and Kirsi Yliniemi for their generous assistance when I moved here and Gunilla Fabricius for providing me with the opportunity to learn so much from teaching undergraduates.

Naturally, the other members of the laboratory are also acknowledged for the help they have given over the years and for the time spent introducing this foreigner to the way of the Teekkari. I would also like to thank

Hessu Viianranta of the workshop for precisely and patiently translating ideas for new experimental devices in to real objects.

At this point I would like to thank the people of Finland for providing my family and me with a comfortable and relatively carefree life during the last five years. It has been a pleasure and a revelation to work in an environment where science and engineering, as well as a healthy family life, are so highly valued and where the aspiration to achieve academic and technical excellence is still alive and well. I only hope that one day I can repay the favour, as well as warn you of the dangers of uncritically adopting too many of our Anglo-Saxon ways.

I am grateful to the British half of my family for continuously reminding that this process should come to a definite end and for providing me with the belief that every value and preconception should be questioned. Special thanks go to my father for introducing me to engineering and programming from such an early age, as well as awakening my wanderlust. I also feel extremely fortunate for the many happy hours I have spent relaxing in the company of my Finnish family, especially that of my two daughters Ulrika and Sofia.

Finally, last but not least, I must thank my wife, Veera, for the last five years. It has been a rollercoaster ride, as always, but enormously enjoyable and rewarding. I could not think of a better companion. You have my eternal gratitude for the sacrifices you made to take such good care of both me and our children during this time.

Espoo, Finland, September 30, 2013,

David Lloyd

Contents

List of Publications

This thesis consists of an overview and of the following publications which are referred to in the text by their Roman numerals.

I David Lloyd, Tuomas Vainikka, Lasse Murtomäki, Kyösti Kontturi, Elisabet Ahlberg. The kinetics of the Cu^{2+}/Cu^{+} redox couple in deep eutectic solvents. *Electrochimica Acta*, $56(2011)4942-4948$, April 2011.

II David Lloyd, Tuomas Vainikka, Sönke Schmachtel, Lasse Murtomäki, Kyösti Kontturi. Simultaneous characterisation of electrode kinetics and electrolyte properties in ionic liquids using a rotating disc electrode. *Electrochimica Acta*, $69(2012)139-145$, March 2012.

III David Lloyd, Tuomas Vainikka, Kyösti Kontturi. The development of an all copper hybrid redox flow battery using deep eutectic solvents. *Electrochimica Acta*, $100(2013)18-23$, March 2013.

IV David Lloyd, Tuomas Vainikka, Markus Ronkainen, Kyösti Kontturi. Characterisation and application of the Fe(II)/Fe(III) redox reaction in an ionic liquid analogue. *Electrochimica Acta*, $109(2013)843-851$, October 2013.

Author's Contribution

Publication I: "The kinetics of the Cu^{2+}/Cu^{+} redox couple in deep eutectic solvents"

The author defined the research plan together with the co-authors, carried out all experimental work and wrote the manuscript.

Publication II: "Simultaneous characterisation of electrode kinetics and electrolyte properties in ionic liquids using a rotating disc electrode"

The author defined the research plan together with the co-authors, carried out all experimental work and wrote the manuscript.

Publication III: "The development of an all copper hybrid redox flow battery using deep eutectic solvents"

The author defined the research plan together with the co-authors, carried out all experimental work and wrote the manuscript.

Publication IV: "Characterisation and application of the Fe(II)/Fe(III) redox reaction in an ionic liquid analogue"

The author defined the research plan together with the co-authors, carried out all experimental work and wrote the manuscript.

Abbreviations and symbols

List of Abbreviations

BMP	1-butyl-1-methylpyrrolidinium
CE	Counter Electrode
CPE	Constant Phase Element
CV	Cyclic Voltammetry
DES	Deep Eutectic Solvent(s)
EIS	Electrochemical Impedance Spectroscopy
EMIM	1-methyl-3-ethylimidazolium
EXAFS	Extended X-ray Absorption Fine Structure
FAB-MS	Fast Atom Bombardment Mass Spectrometry
FRA	Frequency Response Analyser
GC	Glassy Carbon
HDE	Hydrodynamic Electrode
IL	Ionic Liquid
Im	Imidazolium
MON	Method Of Nicholson
QRE	Quasi Reference Electrode
RDE	Rotating Disc Electrode
RE	Reference Electrode
RFB	Redox Flow Battery
TFSI	bis(trifluoromethylsulfonyl)imide
VFT	Vogel-Fulcher-Tammann
WE	Working Electrode
WJE	Wall-Jet Electrode
WTE	Wall-tube Electrode

Standard subscripts

W	pertaining to a Warburg Element
O	pertaining to the oxidised form
R	pertaining to the reduced form
F	pertaining to a Faradaic process
CPE	pertaining to a Constant Phase Element

Roman symbols

a	area of WE
C	concentration
C_{bulk}	concentration in bulk
C_{dl}	capacitance of WE/electrolyte interface
D	diffusion coefficient
f	F/RT
F	Faraday constant
E	potential of WE
$E^{0'}$	formal potential
E_{eq}	equilibrium potential
E_{obs}	potential measured between WE and RE
ΔE_{peak}	potential difference between two peaks
E_{a}	activation energy
I_{K}	kinetic current
I_l	limiting current
I_0	exchange current
I_{p}	peak current
j	imaginary unit ($j^2 = 1$) or current density
k_{B}	Boltzmann constant
k_{f}	forward rate constant
k_{b}	backward rate constant
k^0	standard heterogeneous rate constant
n	number of electrons transferred
n_{f}	frequency exponent of CPE
N	molar flux

Q_{charge}	charge transferred to cell during charging
$Q_{\text{discharge}}$	charge transferred to cell during discharging
Q_{theory}	theoretical charge capacity of cell
r_{H}	hydrodynamic radius
r_{T}	radius of nozzle opening
R	ideal gas constant
R_{ct}	charge transfer impedance
R_{s}	solution resistance
T	temperature
T_{g}	glass transition temperature
T_0	ideal glass transition temperature
v	velocity or scan rate
V_{f}	volumetric flow rate
x	distance from electrode surface or mole fraction
Y_0	standard admittance of a CPE
Z	impedance
$Z_{C_{\text{dl}}}$	impedance of C_{dl}
Z_{Im}	imaginary component of impedance
Z_{Re}	real component of impedance
$Z_{\text{W,s}}$	impedance of short-circuit Warburg element

Greek symbols

α	charge transfer coefficient
δ	thickness of Nernst layer
η	overpotential or dynamic viscosity
η_{E}	Energy efficiency of discharge process
η_{Q}	Coulombic efficiency of discharge process
κ	conductivity of electrolyte
Λ	molar conductivity
ν	kinematic viscosity
ω_{EIS}	angular frequency of excitation during EIS
ω_{RDE}	angular frequency of rotation of RDE
Ψ	dimensionless number relating kinetics, mass transport and experiment duration
ρ	density

1. Introduction

Ionic liquids (ILs) are a class of materials that currently enjoy great popularity in the scientific literature due to their unusual physical properties. Some ILs remain liquid until well below the freezing point of water, while still exhibiting negligible vapour pressure at ambient conditions and a decomposition temperature of 200 °C [1]. Some also show no miscibility with water, allowing the development of novel separation processes [2]. In addition, some ILs are so stable with respect to electrochemical decomposition, that reactive metals, such as sodium and lithium can be deposited from them [3]. It is this last property that initially motivated the work performed in this thesis.

The first major problem encountered is that the majority of ILs are prohibitively expensive and likely to remain so in the foreseeable future. This precludes their use in anything other than niche applications. For this reason the subject of this thesis is an IL based on the combination of ethylene glycol and choline chloride, which is known as ethaline. Ethaline exhibits similar physical and chemical properties to ILs based on the chloride anion, is stable under ambient conditions, cheap and biodegradable. It the most conductive and least viscous member of a group of materials known as deep eutectic solvents (DES) [4]. The status of DES as ILs is ambiguous due to the absence of any conclusive evidence that the chloride ion forms a discrete anionic complex with hydrogen bond donors, such as ethylene glycol. However, if one can look past this one weakness, then in all other respects they have more in common with chloride based ILs than traditional molecular solvents.

Since ethaline is not particularly stable with respect to electrochemical decomposition the second major problem encountered in this work was

what metal could be studied without the added complication of this decomposition reaction. Based on the experience of the supervisor it was decided to study copper and this immediately proved to be an excellent system to test a range of electrochemical techniques.

However, since the electrodeposition of copper from water is so simple the third problem encountered was what work could usefully be done? When the pioneering electrochemical studies carried out by the groups of Hussey [5], Osteryoung [6] and Wilkes [7] in the early nineteen-eighties to characterize the electrochemistry of a range of elements in chloroaluminate ILs was compared with contemporary electrochemistry using modern ionic liquids it became clear that the quantitative characterization of the key parameters that describe electrochemical processes, and which allow direct comparison of one system with another, has largely fallen out of fashion.

The common trend in modern research is to perform simple cyclic voltammetric measurements to identify the approximate location of some processes, followed by deposition and characterization of the deposit formed [8][9]. Much greater emphasis is placed on studying the morphology, crystallographic orientation and composition of the deposit than the process by which it is arrived at.

Since there has also been significant progress in the range of electroanalytical techniques available it seemed a reasonable objective to perform studies that would utilize these techniques to quantitatively compare an electrochemical process in ethaline and the other ILs. This is the work contained in publication I. This demonstrated the similarity between ethaline and chloride-rich ILs with regards to the copper complex formed and the properties of the redox reaction between Cu^{+} and Cu^{2+}.

Viscosity and conductivity are two of the most important properties of any ionic liquid. This is because in this respect ionic liquids are inferior to molecular solvents at ambient conditions, often by many orders of magnitude [10]. This is a crucial weakness, since the technical application of ionic liquids would be limited to a few niche processes if these properties could not be improved, at least partially, by increasing temperature. The characterization of viscosity as a function of temperature is a non-

trivial activity for chloride rich ionic liquids due to the corrosivity of ILs towards the majority of materials used to manufacture rheometers. For this reason, techniques that utilize electrochemical measurements at the rotating disc electrode (RDE) to quantify both conductivity and viscosity of ethaline over a range of temperatures were developed. In addition the use of the RDE to both simplify and improve the accuracy of methods to characterize the properties of electrochemical processes is shown. This is the work presented in publication II.

At this point the work undertaken was solely of interest to members of the academic community interested in electroanalytical techniques or electrochemistry in ILs, with no obvious technical utility. Additionally, with the benefit of a few years experience, the disappointing realization was made that ILs are often, in the opinion of the author, overhyped as media for electrodeposition. This is because the majority of metals can be deposited with significantly less cost and greater efficiency from water (the ultimate green solvent) [11]. Additionally, the deposition of reactive metals, such as lithium or aluminium, from ILs demands scrupulous purity of the liquid and operation under an inert atmosphere. These are essentially the same demands placed on identical processes when they were performed in haloaluminate ILs some sixty years ago by Hurley and Weir [12] or in modern processes based on organic solvents, such as the Sigal process to deposit aluminium on steel from toluene [13]. If the current generation of ILs do not solve the problems that have prevented the development of commercially competitive electrodeposition processes based on haloaluminates, then what hope do they have of succeeding? This question appears to be largely overlooked by the parts of the IL community studying electrodeposition applications.

The problem of what might possibly be a useful electrochemical application for ILs was answered when the fields of redox flow batteries (RFBs) and molten salt batteries were examined. Molten salt batteries, such as the Zebra battery, are energy storage systems exhibiting similar performance to lithium batteries [14]. Since ILs are simply molten salts that happen to be liquid below 100 °C it is eminently reasonable to imagine that they could be utilized in a low temperature molten salt battery. As the mass transport properties of ILs are poor at lower temperatures, such a battery benefits substantially from the introduction of convection,

which naturally leads to construction of an RFB. In publication III this was demonstrated for the first time in any DES by applying the same redox reaction that had been studied in publication I and II.

RFBs and molten salt batteries are potentially major building blocks in the development of a sustainable energy system due to their scalability and reliable performance over many thousands of cycles [15]. The amount of materials required to achieve significant balancing of the electricity grid dwarves any previous application of battery technology [16]. The problem of materials availability then arises. For this reason in publication IV the electrochemistry of iron and iron chloride salts was studied in ethaline and applied in a RFB. This showed that for chloride based systems the transition from a nominally aqueous system to a DES did not change any of the fundamental characteristics of the system.

In summary, this thesis illustrates a range of techniques to characterize the parameters that quantitively describe the performance of electrochemical processes. The utility of these methods as a means to understand the problems that limit performance in RFBs is examined. The similarity between DES and chloride-rich ILs is amply demonstrated. Finally, the successful development of a range of RFB chemistries based on ethaline is shown.

2. Ionic liquids and Deep Eutectic Solvents

The class of materials known as ionic liquids (ILs) are generally defined as highly dissociated salts, containing only discrete cations and anions, that are molten below 100 °C [17]. A typical ionic liquid has an extremely low volatility, compared to water or typical organic solvents. It is likely that materials which fit such a definition have been known to at least part of the scientific community throughout modern times. However, the generally accepted point at which the field is considered to begin is the report by Paul Walden of the conductivity and viscosity of a material he termed an 'ionic liquid' in 1914 [18].

The liquid he studied, ethyl ammonium nitrate, can be formed by the reaction of nitric acid with ethyl amine, it is shown in figure 2.1. The ammonium cation formed contains numerous hydrogen substituents and therefore the first IL to be reported belonged to a group of ILs known as protic ionic liquids.

2.1 Haloaluminates

The next phase was the development of ILs based on anionic haloaluminate complexes. Initially, bromide and chloride salts were both studied [12]. However, the field rapidly narrowed to consider only the chlorocomplexes. Simultaneously, progress was made in the development of organic cations with exceptional electrochemical stability, such as the alkyl substituted imidazolium family. These ionic liquids can be prepared by reacting a suitable chloroalkane with an alkylimidazole to form an imidazolium chloride (ImCl) [19]. This is followed by combination with varying amounts of $AlCl_3$ to form a range of complexes, as shown in equations 2.1 and 2.2.

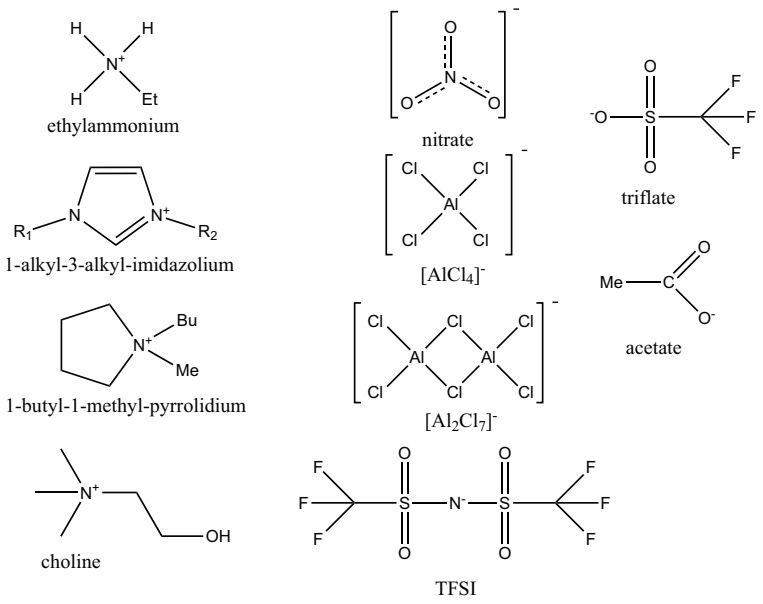

Figure 2.1. Structure of the various cations and anions discussed in this chapter

$$\mathrm{AlCl_3} + \mathrm{ImCl} \rightleftharpoons \mathrm{Im^+} + [\mathrm{AlCl_4}]^- \tag{2.1}$$

$$2\,\mathrm{AlCl_3} + \mathrm{ImCl} \rightleftharpoons \mathrm{Im^+} + [\mathrm{Al_2Cl_7}]^- \tag{2.2}$$

In the chloroaluminate system three anionic species are relevant. They are $\mathrm{Cl^-}$, $[\mathrm{AlCl_4}]^-$ and $[\mathrm{Al_2Cl_7}]^-$. The relative prevalence and identity of each as a function of composition has been established using a range of techniques such as NMR spectroscopy and potentiometric titration [20]. A typical dependency is shown in figure 2.2.

This correlates well with the variation in the physical properties of the system, such as melting point, T_m, shown in figure 2.3. Chloroaluminate systems with an excess of chloride ions, corresponding to a mole fraction of $\mathrm{AlCl_3}$, $x_{\mathrm{AlCl_3}}$, greater than 0.5 are considered to be Lewis acidic, i.e. they are capable of accepting a pair of electrons. Those with $x_{\mathrm{AlCl_3}}$ less than 0.5 are Lewis basic. In the opinion of the author it is simpler to talk about a chloride rich or a chloride poor system to distinguish between the basic or the acidic situation.

In addition to melting point, the prevalent anionic chloroaluminate complex also changes the cathodic limit of the liquid. In the case of acidic

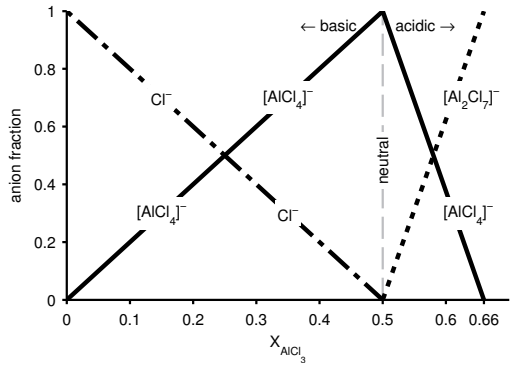

Figure 2.2. Relative prevalence of the various anionic complex in the 1-methyl-3-ethylimidazolium (EMIM) Cl - $AlCl_3$ system. The chloride rich 'basic' region and the chloride poor 'acidic' region, as well as the neutral compostion are shown. Adapted from [7]

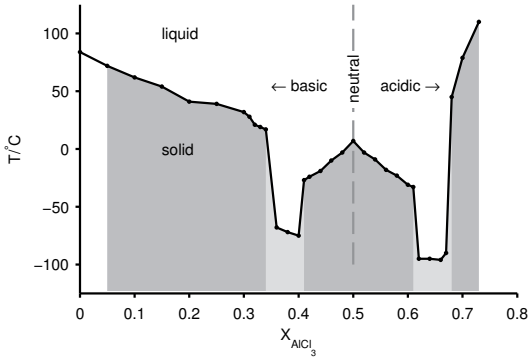

Figure 2.3. Phase diagram of the EMIM Cl - $AlCl_3$ system. The chloride rich 'basic' region and the chloride poor 'acidic' region, as well as the neutral compostion are shown. The darker shaded areas indicate the regions where a typical solid-liquid transition is observable, the lighter shaded areas indicate regions where a glass transition is observed. Adapted from [7]

chloroaluminates deposition of metallic aluminium is possible. The ability to deposit aluminium, or even more electronegative materials from Lewis basic chloroaluminates, has resulted in this class of liquids remaining a subject of ongoing interest to the IL community.

2.2 Air and moisture stable ionic liquids

The current boom in ionic liquids research was initiated by the recognition that chloroaluminate anions were a limiting factor, as their reactivity towards both oxygen and water required experiments to be performed under an inert atmosphere. Their substitution by air and moisture stable

anions, such as acetate or triflate, allowed the study of ionic liquids by a wider range of scientists and their application in a much broader range of processes, such as biomass treatment.

The development of ever more exotic fluorine substituted anions, such as trifluorosulfonylimide (TFSI) shown in figure 2.1, has led to the development of hydrophobic ionic liquids. These ILs are immiscible with water, although they will show some mutual solubility [21]. It is worth noting at this point that many materials that were widely used prior to the popularity of ionic liquids are in fact hydrophobic ionics liquids. A prime example is trioctylmethylammonium chloride (Aliquat 336), which is a phase transfer agent widely used in organic chemistry since 1971 and which is immiscible in water, inspite of the chloride anion [22].

2.3 The pros and cons of Ionic Liquids

At this point is seems appropriate to clearly identify the four main problems which limit the application of ionic liquids in industrial electrodeposition processes.

Firstly, the stability of modern ionic liquids against reaction with air and water does not necessarily mean they can be applied successfully without the use of a protective atmosphere. Water and oxygen can both be absorbed and will interfere with the electrodeposition of a reactive metal [23, 19].

Secondly, ionic liquids have poor transport properties compared to molecular solvents, such as water. For instance, they are at least an order of magnitude more viscous than molecular solvents, which leads to slow transport of diffusing species in the case of a heterogeneous reaction, such as electrodeposition [19]. Additionally, their conductivity is typically two orders of magnitude lower than common aqueous electrolytes. This negatively impacts electrodeposition processes, since such an electrolyte will have poor throwing power (which leads to uneven deposition) and give higher Ohmic losses than a molecular solvent at a similar current density.

Thirdly, their status as ‘green solvents’, which is apparently derived entirely from their low vapour pressure, is unfounded. They are often toxic

and the means for their eventual disposal is largely unknown [24].

A final problem is that they are expensive, especially if a high purity is required. They are also only available in small quantities, with the ton scale being a typical upper limit.

Inspite of these problems there are some noteworthy examples of commercially successful processes and technically impressive electrodeposition studies. An example of the former is the BASIL process to produce alkoxyphenylphosphines [25].

An example of an impressive electrodeposition process is the preparation of Si, Ge and Si-Ge alloys exhibiting a tuneable bandgap [26]. Such a process could, perhaps, revolutionize the manufacture of solar panels, by allowing the preparation of similarly large monolithic silicon solar panels as was achieved over ten years ago for cadmium-telluride panels [27]. Alternatively, it could allow the manufacture of large, energy-efficient lighting panels.

2.4 Deep Eutectic Solvents as analogues of Ionic Liquids

Given the limitations to mainstream ILs outlined above, there is a clear motivation for the development of ILs, or materials with similar physical and chemical properties, that are based on compounds that are biodegradable, affordable and available in large quantities with high purity.

The first such material to gain widespread interest was the combination of trimethylethanolamine (choline) chloride and urea [28]. The structure of choline is shown in figure 2.1. This material and a range of similar materials where urea is substituted by carboxylic acids [29] or glycols [4] were developed by Abbott and coworkers. Taken together these are referred to as deep eutectic solvents (DES).

The DES used in this thesis is a mixture of choline chloride and ethylene glycol, combined in a 1:2 molar ratio, which is known as ethaline. Ethaline has the lowest viscosity and highest conductivity of all DES reported to date and has been studied by a number of groups for over five years [30, 31, 32].

Since ethylene glycol is a liquid at ambient conditions and no studies detailing the liquid-solid phase transition for this DES have been published, there is some ambiguity as to whether the stoichiometry commonly used corresponds to a eutectic composition. Additionally, during electrochemical studies using transition metal chloride salts the solute can significantly compete with ethylene glycol in the complexation of chloride. At this point the system can become a ternary eutectic.

While the initial tendency was to label these materials as ionic liquids, it would appear that after a period of grace the academic community no longer tolerates such sloppy classification. The popular hypothesis was that the chloride anion forms a discrete hydrogen bonded complex with the other component of the mixture. The primary evidence to support this was based on mass spectroscopy measurements using fast ion bombardment (FAB-MS) [33]. The comparability of the bombarded state to bulk conditions was always questionable and recent work by Seddon has shown that FAB-MS results are likely to provide little or no indication of the actual state in an unperturbed liquid [34]. The structure of DES at the molecular level is therefore unknown and there is no evidence to suggest that they are essentially different from any other mixture of a polar molecular solvent and a chloride salt.

Thankfully, parallel studies were underway at this laboratory to investigate the properties of the copper chloride system in a widely accepted IL, namely butylmethylpyrollidinium (BMP) TFSI [35, 36]. The similarity exhibited by the complexes formed in BMP TFSI and the DES studied here, as well as the comparability with earlier reports for chloroaluminate ILs, persuaded the author that even if DES are not strictly speaking ILs, they are sufficiently similar to be considered analogues of ILs and equally worthy of study.

Work by other authors has demonstrated the successful deposition of nickel [37], zinc [38], copper [31], iron [39] and chromium [40] using DES. It is worth noting that all these elements can be deposited with relative ease and greater efficiency from aqueous solutions [11].

2.5 Transition metal complexes in chloride rich ionic liquids and deep eutectic solvents

Although the chemistry of the chloroaluminate system is by far the most widely reported, other transition metal halides were also studied at around the same time, these include $CuCl_2$, $FeCl_3$ and $ZnCl_2$. These all form a variety of chlorometallate anions. In the case of chlorocuprates the dominant anionic complex was shown by Scheffler and Thompson to be $[CuCl_4]^{2-}$ [41]. Amuli et al. showed the presence of both $[CuCl_4]^{2-}$ and $[CuCl_3]^{-}$ anions in trimethyl phosphate [42]. The $[CuCl_4]^{2-}$ complex is also formed in concentrated HCl solutions [43]. Naturally, a related group of chlorocuprate complexes also exist for the Cu(I) oxidation state. These have been shown by Bolkan and Yoke to be $[CuCl_3]^{2-}$ and $[CuCl_4]^{3-}$ [44].

Sitze et al. are among a number of authors to study the formation of chloroferrate complexes [45]. They reported the formation of ionic liquids based on both the divalent $[FeCl_4]^{2-}$, trivalent $[FeCl_4]^{-}$ and $[Fe_2Cl_7]^{-}$ complexes. The latter complex forms when an excess of $FeCl_3$ is present in the liquid. Chloroferrate ILs based on the combination of BMIM Cl and $FeCl_3$ have been shown by Angell to possess some of the best transport properties reported for ILs, exceeding those of liquids with an identical cation and a modern, fluorinated anion [10, 46]. Abbott et al. have also reported the preparation of a chloroferrate ionic liquid based on the same choline cation used in DES, although this only forms a liquid at 65 °C [47].

Abbott et al. have recently utilized Extended X-ray absorption fine structure (EXAFS) analysis to demonstrate that in ethaline zinc is coordinated by four chloride ions [38], this suggests a $[ZnCl_4]^{2-}$ complex. This is compatible with work on choline based chlorozincate ILs, where a low melting stoichiometry occurs at the 2:1 molar ratio of $ZnCl_2$ to ChCl [47]. Liu et al. have shown using DSC that the lowest melting stoichiometry is the 3:2 ChCl:$ZnCl_2$ ratio, corresponding to a 2:1 mixture of $[ZnCl_4]^{2-}$ and $[Zn_2Cl_6]^{2-}$ anion complexes [48]. Estager et al. have shown that the $[ZnCl_4]^{2-}$ complex dominates in chloride rich media [34], however as the $ZnCl_2$ content increases a range of polyatomic complexes, including the $[Zn_2Cl_6]^{2-}$ anion, are formed.

3. Experimental techniques in ionic liquids and deep eutectic solvents

Although the same techniques are applicable in ILs as in any other electrolyte system, the poor conductivity of ILs, compared to aqueous electrolytes, means that particular care has to be paid to the issue of Ohmic losses.

Irrespective of the electrolyte, the primary motivation when applying these experimental techniques is to quantitatively describe the properties of processes and devices, e.g. electrodeposition throughput or battery performance, in such a way that we can understand what will limit performance and where effort can best be spent to achieve useful improvements.

As mentioned in the introduction, the range of quantitative electrochemical techniques which had been utilized in the study of DES were rather limited. Therefore a significant part of this thesis describes the work undertaken by the author to successfully apply additional techniques. Work was also undertaken to develop new techniques, which are also described here.

A typical experimental technique consists of three parts:

Conceptual Framework: This is the generalized image we have of how a system functions. Often it appears indistinguishable from the mathematical description. The important aspect of the framework is that it is general, i.e. it is common to a wide range of techniques. Often these descriptions assume a dogmatic status. A prime example of this is diffusion, which can so often be successfully described by the model of Fick that the two become almost inseparable. The same conceptual framework may serve other purposes too, such as indicating how we might

use the physical parameters determined using an experimental technique to model the properties of a hypothetical device or process.

The relevance of the framework, when describing an experimental technique, is that it often includes assumptions or simplifications that limit the range of situations over which a technique can yield reliable results. For instance, diffusion can only be accurately described by the model of Fick for dilute systems. This is particularly important during the design of experiments.

Theory: This is typically a simple mathematical description of how the system responds to the application of a particular technique. This also indicates how the technique can be used to determine some parameter of the system, such as the diffusion coefficient of a species, from the observed response.

Instrumentation: This consists of the hardware and software used to perform the experiment. Since the successful application of a technique is entirely dependent on the selection and use of appropriate instrumentation this is a not a trivial element. Given the key role of software in modern electrochemical instrumentation, it could also be argued that the computational methods used to process the data collected during an experiment is also part of the instrumentation, since it can also significantly bias the outcome.

3.1 Conceptual Framework

The techniques applied in this work generally deal with the quantification of one or more of the processes that take place during a heterogeneous electrochemical reaction at an electrode surface. As shown in figure 3.1, there are three stages in a heterogeneous electrochemical reaction: transport of dissolved species to the surface, transfer of electrons across the interface and transport of products away from the surface.

In this thesis Fick's first law is used to describe the transport of matter to and from the electrode. This model assumes that the species being studied is present in a much lower concentration than the supporting

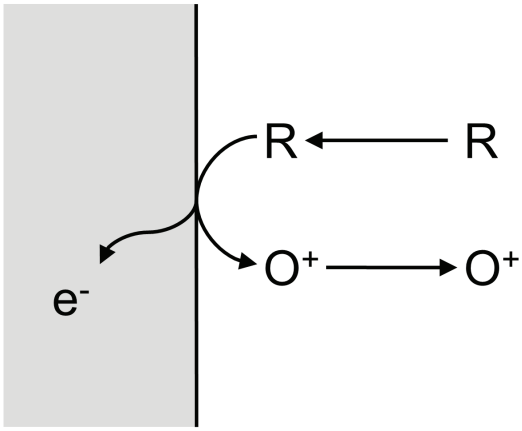

Figure 3.1. A simple heterogeneous reaction at an electrode surface

electrolyte, which in this case is the DES itself. Otherwise the effect of migration, due to the presence of an electric field in the vicinity of the electrode surface, needs to be taken in to account. For the example shown in figure 3.1 the molar flux density of species R, N_{R}, is related to the local gradient in the concentration of R, C_{R}, by its diffusion coefficient, D_{R}, as shown in equation 3.1 where x is the distance from the electrode surface.

$$N_{\mathrm{R}} = -D_{\mathrm{R}} \frac{dC_{\mathrm{R}}}{dx} \tag{3.1}$$

Naturally, the rate at which a species can transfer through an electrolyte is related to the dynamic viscosity, η. The common way in which to express this is in the form of an effective hydrodynamic radius, r_{H}, which is also known as the Stokes radius. This approximation assumes that at the microscopic level the electrolyte is a perfectly homogeneous medium and the diffusing species perfectly spherical. While neither assumption is plausible for ILs or DES this appears to be the best model available and results in the Stokes-Einstein equation given below.

$$D = \frac{k_{\mathrm{B}} T}{6\pi\eta r_{\mathrm{H}}} \tag{3.2}$$

In equation 3.2 k_{B} is the Boltzmann constant and T is temperature. The conversion of R to O^+, shown in figure 3.1 and equation 3.3, involves the transfer of an electron from R to the electrode.

$$\mathrm{O}^+ + \mathrm{e}^- \underset{k_{\mathrm{b}}}{\overset{k_{\mathrm{f}}}{\rightleftharpoons}} \mathrm{R} \tag{3.3}$$

The energy required to add or withdraw an electron to or from the electrode is homogeneous throughout for good conductors and equals the work

function of the electrode. This simple fact means that the Gibbs energy of the reaction depends on the electrode potential and we can drive the reaction in either direction by adjusting the electrode potential. The simplest and most common model to describe this dependency is the Butler-Volmer model (B-V model). In the B-V model the two rate constants, k_{f} and k_{b} in equation 3.3, depend exponentially on the difference between the electrode potential, E, and the formal potential, $E^{0'}$, of the reaction as shown in equations 3.4 and 3.5.

$$k_{\mathrm{f}} = k^0 \exp(-\alpha f(E - E^{0'})) \tag{3.4}$$

$$k_{\mathrm{b}} = k^0 \exp((1-\alpha) f(E - E^{0'})) \tag{3.5}$$

In equations 3.4 and 3.5 k^0 and α are the heterogeneous rate constant and charge transfer coefficient of the reaction respectively and $f = F/RT$. F is the Faraday constant and R is the ideal gas constant. k^0 indicates how facile the reaction is, while α indicates whether the forward or backward reaction is more facile. If no other electrochemical reactions occur at the electrode surface then all the current due to Faradaic processes, I_{F} will be attributable to the reaction shown in 3.3. Simultaneously the molar fluxes of R and O will be equal and opposite and also proportional to I_{F}, as shown in equation 3.6.

$$\begin{aligned} \frac{I_F}{nFA} &= -D_{\mathrm{R}} \frac{dC_{\mathrm{R}}}{dx} = D_{\mathrm{O}} \frac{dC_{\mathrm{O}}}{dx} \\ &= k_{\mathrm{b}} C_{\mathrm{R}} - k_{\mathrm{f}} C_{\mathrm{O}} \\ &= k^0 \left(C_{\mathrm{R}} \exp((1-\alpha) f(E - E^{0'})) - C_{\mathrm{O}} \exp((-\alpha) f(E - E^{0'})) \right) \end{aligned} \tag{3.6}$$

Where n is the number of electrons transferred. The ability to both control and quantify the rate of a chemical reaction by adjusting the electrode potential and measuring the electrical current respectively is a uniquely powerful aspect of electrochemistry, with only photochemistry showing remotely comparable ease of control.

A complicating factor is that charging of the electrode surface occurs in parallel to the electrochemical reactions taking place. This does not involve transfer of electrons across the surface, simply rearrangement of charged species in solution resulting in a change of the charge on the electrode. Because it does not involve charge transfer across the interface it is a rapid process which can essentially be treated as charging of a capacitor

with capacitance C_{dl}.

Finally, for both these processes to take place there needs to be a complete electrical circuit. This requires a second electrode and for current to pass through the electrolyte. Since a finite separation exists between the reference point in the circuit against which we measure the electrode potential and the electrolyte possesses a finite conductivity, κ, this manifests itself as a resistance, R_{s}. For a flat, disc shaped electrode, set in an inert surface, with the reference point set sufficiently far from the electrode surface, Newman has shown that R_{s} is related to κ by the relation shown in equation 3.7, where a is the electrode area.

$$R_{\mathrm{s}} = (4\kappa a)^{-1} \tag{3.7}$$

As was mentioned in the introduction, the transport properties of ILs are relatively poor at ambient conditions. A model to describe the manner in which these properties depend on temperature is therefore desirable. The most widely used model is that developed by Arrhenius, which is shown in equation 3.8.

$$k = A \exp\left(\frac{-E_{\mathrm{a}}}{RT}\right) \tag{3.8}$$

This assumes that the rate at which a given process takes place, k, is proportional to the thermal energy of the system, RT, and a fixed activation energy, E_a. A is the preexponential factor. The physical significance of A depends on both the phenomena being studied and the choice of conceptual framework. In the case of the Butler-Volmer model, which is based on the simplest form of transition state theory, A can be further interpreted in terms of the Eyring equation. Such an interpretation requires that additional information regarding the partition function of the activated complex is available, typically from spectroscopic measurements and that such a simple model is appropriate. In this work the Arrhenius model has been found to be highly satisfactory and allows a simple comparison of the effect of changing temperature on different processes. The alternative Vogel-Fulcher-Tammann (VFT) equation is popular for ILs and its use is certainly justifiable on strictly theoretical grounds [46]. The VFT equation is shown in equation 3.9.

$$k = A \exp\left(\frac{-E_{\mathrm{a}}}{R(T - T_0)}\right) \tag{3.9}$$

Since the VFT equation introduces an additional parameter, in the form of an ideal glass transition temperature, T_0, to the Arrhenius equation it should be no surprise that it may provide a better fit of experimental data. However, in itself this is no proof that its choice is a valid one. Ideally, measurements should be performed over a wide range of temperatures, especially including the region close to T_0, where the difference with the Arrhenius model is most strongly pronounced. T_0 itself is not a directly observable property of a liquid, although it should be located below the observable glass transition temperature, T_g. The use of the VFT equation makes it extremely difficult to compare the temperature dependency of processes, unless they are all assumed to have the same value of T_0.

This is one example of the choice that needs to be made during interpretation of experimental results. More sophisticated and accurate models certainly exist for all parts of the framework given above, but these are often purely of interest to a minority. What the majority want to do is to compare the behaviour of different systems with the least effort possible, this leads naturally to the emergence of a dominant conceptual framework. As time passes, the literature becomes dominated by results which have been interpreted in terms of this framework and attempts to interpret results using a new framework can then become problematic, as the parameters a new framework produces will not necessarily be readily comparable with those of the dominant framework.

3.2 Instrumentation

3.2.1 Potentiostat

The instrument at the heart of the experimental system used in this thesis was a Solartron 1286 potentiostat (SL1286). A potentiostat is fundamentally an analogue device that allows the potential at one electrode to be controlled with great precision relative to a second electrode. These are the working electrode (WE) and reference electrode (RE) respectively. Importantly, the potentiostat ensures that minimal current passes through the RE. Instead the current passing through the WE is matched by an equal and opposite current passing through a third electrode, which is the counter electrode (CE). A potentiostat also has a range of resistors

which it can rapidly switch between to monitor current with high precision. A typical example is the SL1286, which extends over a range from 2A to 2μA, which is six orders of magnitude. The ability to sample over such a wide dynamic range within one experiment is another remarkable aspect of electrochemical measurements.

To minimise the effect of Ohmic losses in the cabling and connectors between the WE and potentiostat the Solartron 1286 provides two separate terminals to connect the WE. One is used to transfer current (labelled WE) and the other is used to monitor the WE potential (labelled RE1). This configuration also allows additional experimental techniques, such as those utilised during DC conductivity measurements.

Additionally, modern potentiostats also allow the compensation of Ohmic losses due to R_{s}. In this thesis this was achieved by measuring the impedance of the system and applying positive feedback. The SL1286 also allows the application of a 10 Hz low pass filter on the current and potential followers. This option was used during slow voltammetric measurements and potential step experiments.

Although it is common to refer to this kind of instrument as a potentiostat, a more accurate name might be 'electrochemical interface'. This is because the same instrument is often used to control current, at which point it functions as a galvanostat. This mode of operation is used extensively during long term studies of RFBs.

3.2.2 Electrochemical cell

With the exception of the conductivity measurements and the RFB measurements the same electrochemical cell was used in all measurements. It consists of a jacketed glass vessel connected to a thermostat. The only unsealed opening in the teflon lid is an 8mm orifice through which the shaft of the WE passes. During operation constant slow purging of the headspace is maintained using nitrogen (99.99%). The volume of electrolyte required to fill this cell is 25 ml. The temperature of the electrolyte was continuously monitored using a glass encased thermocouple. The counter electrode was a platinum (Pt) spiral and the reference electrode was a Pt wire quasi reference electrode (QRE), these were connected to the potentiostat by sealed contacts passed through the teflon lid.

In addition to the QRE, an Ag/AgCl reference was prepared and used to quantify drift in the reference potential provided by the QRE. This electrode was prepared by anodizing a silver wire (1 mm diameter) in 0.1 M HCl followed by rinsing with ethanol and drying with a nitrogen stream. This was then fitted in a glass capillary to prevent contamination of the electrolyte due to corrosion of metallic silver by oxidising species in the bulk solution. Once the cell was assembled and filled with electrolyte the capillary was filled with the same electrolyte present in the bulk.

The working electrodes were RDE tips (either glassy carbon (GC) or platinum, Pine Research Instrumentation). These consist of a disc electrode (5mm diameter) with a Teflon sheath. Prior to performing a batch of experiments these were polished by first sanding with carbimet paper (600 grit, Buehler) and then 1 and 0.05 μm alumina paste on a microcloth (Buehler). All electrodes were ultrasonicated in distilled water and absolute ethanol prior to use.

3.2.3 Control/data processing system

To perform a typical electrochemical experiment requires some kind of waveform generator and method to log the response of the electrochemical system to the waveform. Traditionally, specialized analogue devices were developed for each technique. However, with the emergence of ever more competent digital electronics this has become simplified, with one device handling an ever greater number of tasks.

During the analogue era, higher level control of the experiment would be performed manually, by adjustment of the specialised waveform generator. The response would be recorded using an x-y plotter, chart recorder or, in the case of high speed techniques, to a storage oscilloscope. Data processing would generally be performed manually. This historical context is relevant, because a significant part of the techniques still popularly applied in electrochemistry were developed during this era and hence they reflect what was technically possible at a point in time when personal computers were not widely available.

In the modern, or digital, era generation of the waveform and storage of the system response is integrated in to the potentiostat. Logging and

analysis of the system response occurs entirely in the digital domain. Typically, the average user only interacts with a highly specialized piece of software. This simplifies operation greatly and potentially allows new methods for studying experimental results. However, it also has two major drawbacks.

Firstly, important details regarding operation of the potentiostat are often hidden from the user. For instance, this means that the properties of the smoothing filters used are not explicitly defined. Instead the user is presented with vague terms such as 'high speed' to indicate the absence of filtering and 'high stability' to indicate that limitation of the potentiostat bandwidth is taking place.

Secondly, the range of experimental methods available, as well as the format in which results are stored, are now defined by the software. Since the majority of potentiostats are controlled by closed-source software, this threatens to lock the electrochemical community in to an environment where the introduction of innovative electrochemical techniques can only occur at the whim of a few manufacturers.

In this thesis, an alternative configuration was used. This combined an analogue era potentiostat (SL1286) with a modern multifunctional DAQ (National instruments 6211 or 6251 DAQ). The attraction of such a system is the freedom it gives to the user to develop their own experimental methods, particularly since it also allows the simple integration of other devices in a unified experimental control system, such as water baths, RDE controllers and a range of transducers for the recording of temperature or electrolyte flow for instance.

3.3 Cyclic Voltammetry

Cyclic voltammetry (CV), is the most popularly applied electrochemical technique by a significant margin. In CV measurements the potential of the working electrode is swept linearly as a function of time between a set of vertices and the resulting current that flows is logged. By varying the rate at which potential is swept information regarding the kinetics of mass transport and the heterogeneous reaction kinetics can determined.

The rate at which potential is swept is referred to as the scan rate, v. This method has its roots firmly in the analogue era since the generation of a triangular waveform is simple and logging of the response can be performed using a simple XY plotter. This measurement type also places relatively minor demands on the capabilities of the potentiostat, provided that the scan rate is sufficiently low.

An example of a sequence of CV measurements is shown in figure 3.2. The experiment commences at 0.2V, sweeps down to -0.6V and then returns 0.2V. During the downward sweep the Cu^{2+} at the surface of the electrode gains an electron and is converted to Cu^{+}, resulting in a cathodic current and a localised decrease in the Cu^{2+} concentration. At a given point the diffusion of Cu^{2+} to the surface becomes limiting and the cathodic current begins to drop, resulting in a peak. During the upward sweep the Cu^{+} formed during the downward sweep is converted back to Cu^{2+}, resulting in an anodic current. Prior to each measurement the electrode is held at the start potential for a period of time equal to three times the duration of the impending measurement. This allows the concentration profiles in front of the electrode to return to their unperturbed state.

In the experiment shown in figure 3.2 v was varied between 0.01 and 50 V/s. To allow presentation of the data in one figure current has been normalised by $v^{1/2}$. This demonstrates that increasing v tends to result in a difference in the potentials at which the peaks occur and an increase in the observed current.

At sufficiently low scan rates the kinetics of the heterogeneous reaction are not apparent. In such a situation the shape of the normalised CV is entirely independent of v. This is one example of what is referred to as reversible behaviour. Reversible behaviour is a feature of the measurement, although the term is often also used, incorrectly, to describe the properties of the redox reaction.

This confusion has arisen from the widespread use of a hypothetical reversible reaction as the basis for a simplified mathematical treatment of electrochemical systems. Such a treatment is both valid and useful, since it allows the development of equations that allow the determination of physical properties from measurements where careful design of the ex-

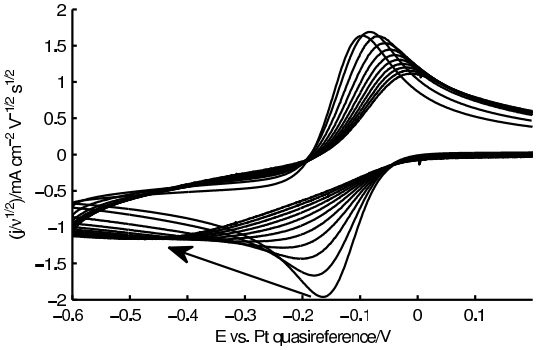

Figure 3.2. Typical results for CV measurements of a 20 mM $CuCl_2$ solution in ethaline at 25 °C at a Pt electrode. Current density is shown normalised by $\sqrt{v}$. The arrow indicates the direction in which the cathodic peak shifts with increasing scan rate. Publication I

periment results in the system exhibiting reversible behaviour.

For a measurement performed under conditions where reversible behaviour is observed an exact analytical relation can be developed that allows the determination of the diffusion coefficient, D, from the height of the first peak, I_p. This is the Randles-Ševčík equation, shown in equation 3.10.

$$|I_\mathrm{p}| = 0.4463 \left(\frac{F^3}{RT}\right)^{1/2} n^{2/3} A D^{1/2} C_\mathrm{bulk} v^{1/2} \tag{3.10}$$

Where C_bulk is the bulk concentration of the species being reduced or oxidised during the first peak. The results of such calculations are shown for the Cu^{2+} and Cu^{+} species in ethaline at a later stage, where they are also compared with other methods.

For a system exhibiting reversible behaviour the separation between the two peaks, ΔE_peak, is independent of v and constant for a given temperature. The existence of reversible behaviour can be validated by measuring ΔE_peak and, if proven, D calculated directly from I_p. For a system where the kinetics are no longer sufficiently facile the peak separation does depend on the scan rate, as is apparent in figure 3.2. This allows determination of the heterogeneous rate constant, k^0. The common method to do this utilises a working curve that was determined numerically by Nicholson and is therefore known as the method of Nicholson (MON) [49]. This provides a relation between ΔE_peak and a dimensionless number, Ψ, which relates the diffusion coefficients of the reduced and oxidised species

(D_{R} and D_{O} respectively) to the kinetics and v, this is given in equation 3.11.

$$\Psi = \frac{(D_{\mathrm{O}}/D_{\mathrm{R}})^{\alpha/2}\, k^0}{\sqrt{\pi D_{\mathrm{O}} f v}} \tag{3.11}$$

Fitting of the experimental data shown in figure 3.2 to this type of working curve is shown in figure 3.3. The fit is only good at high values of Ψ, this corresponds to slow scan rates. The limiting case of reversible behaviour is apparent here. In the working curve prepared by Nicholson, the largest value of ΔE_{peak} given is 212 mV, this range is sufficient to determine k^0, without straying in to the region where ΔE_{peak} shows an appreciable dependency on the value of α. This allowed Nicholson to avoid having to present a table of working curves for differing values of α.

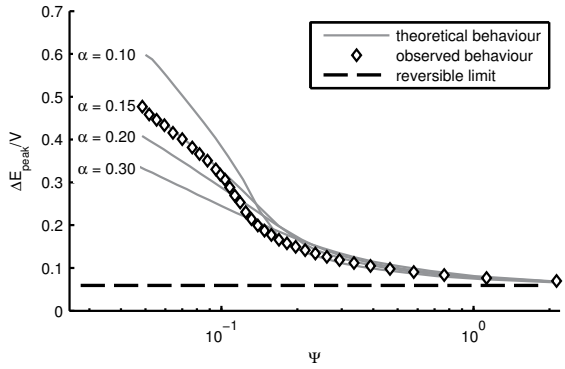

Figure 3.3. Fitting of ΔE_{peak} from the voltammetric data shown in figure 3.2 to simulated working curves. Publication I

However, this introduces a bootstrapping problem, since α is a parameter required to determine Ψ. For this reason as part of this thesis, an extended range of working curves were calculated to low values of Ψ and for differing values of α. In the case of large deviations of α from 0.5 in either direction ΔE_{peak} was found to increase rapidly with decreasing Ψ and provide no obvious discriminating power. For this reason the ratio of the two peak currents, $I^0_{\mathrm{p,a}}/I^0_{\mathrm{p,c}}$ was simulated as a function of both Ψ and α and found to have a distinctive dependency, as shown in figure 3.4. This indicates that the value of α is 0.2. The results of work to determine the value of k^0 for the Cu^{+}/Cu^{2+} reaction are presented in section 3.6.

A problem with this approach is that the use of working curves is only efficient if they are applicable across a wide range of experimental condi-

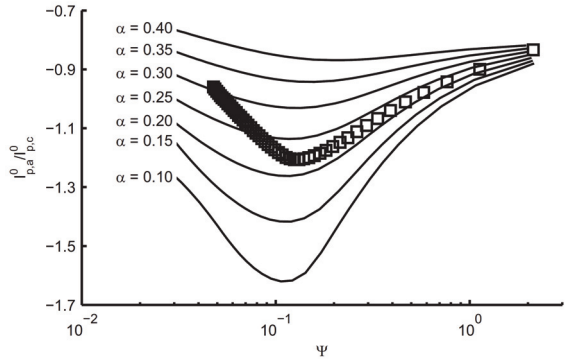

Figure 3.4. Fitting of $I^0_{\mathrm{p,a}}/I^0_{\mathrm{p,c}}$ from the voltammetric data shown in figure 3.2 to simulated working curves. Publication I

tions. In the case of the method of Nicholson the curve used is essentially valid for all systems exhibiting quasireversible kinetics at 25 °C. The use of $I^0_{\mathrm{p,a}}/I^0_{\mathrm{p,c}}$ in contrast is highly dependent on the potential at which the direction of the sweep is switched. The working curves presented here would therefore require recalculation for every set of experimental conditions, although even without recalculation they provide a reasonable initial indication of α. Recalculation is a relatively trivial task with modern computers.

However, at such a point it would seem more appropriate to instead utilise numerical techniques, such as those developed by Osteryoung[50] and extended recently by Vainikka [36], to perform fitting of the complete voltammogram. Such techniques are more readily expandable to include a wider range of phenomena, such as homogeneous reactions, and offer inherently better precision since they consider the entire observed response, rather than a single crude observable, such as ΔE_{peak}.

Experimental constraints to the use of Voltammetric techniques
Traditionally, a discrete analogue ramp generator unit was used to perform CV measurements. The majority of modern potentiostats have an internal digital waveform generator and hence no capability to produce a smooth analogue waveform. Instead a staircase waveform is generated. Provided the step size is sufficiently small, the response of the system is close to that observed for a linear sweep and the approximation is valid.

Vainikka has shown that for a step size of 1 mV, the error in the peak height is 6% for a staircase waveform vs. a linear waveform [51], for a

10 mV step the error in the peak height is already 20%, which is clearly unacceptable if D is to be calculated with good accuracy. The accuracy of staircase voltammetry also depends on the current response being sampled at an appropriate point within the step, with sampling at 0.3 of the step interval giving the closest agreement [51]. While the approximation between staircase and cyclic voltammetry may be shown to be close under certain conditions during simulations, the actual error made during real experiments is inherently uncertain.

One potential benefit of using a staircase waveform is that, provided the time constant of the circuit formed by R_{s} and C_{dl} is sufficiently small, charging of C_{dl} will have occured before the current is sampled and is then not apparent in the response observed. Finally, it should be noted that all the methods presented in this section depend on the complete compensation of the Ohmic losses if the accuracy of the parameters determined are of any interest.

3.4 Potential step techniques

This section discusses a robust and simple method to determine diffusion coefficients. Instead of linearly sweeping potential from a point at which the concentration profiles in front of the electrode are flat, this technique works by taking a large potential step, to a point where the surface concentration of the species being studied rapidly drops to zero. In this way the effect of electrode kinetics is entirely sidestepped and a precise analytical solution to the resulting mass transport problem for a stagnant film can be developed. This is the Cottrell equation, shown in equation 3.12, which indicates that the observed current is proportional to $t^{-1/2}$, where t is the time elapsed since the step was initiated.

$$|I(t)| = \frac{nFAD^{1/2}C_{bulk}}{\pi^{1/2}t^{1/2}} \tag{3.12}$$

The reliability and experimental simplicity of this technique is due to the fact that for sufficiently large potential steps the issue of Ohmic losses, which plagues traditional techniques based on CV measurements in ILs, is also avoided. Examples of experimental data, and fitting, for the $[FeCl_4]^-$ complex studied in Publication IV are shown in figure 3.5.

After an initial period of 0.5 s, during which the capacitive current due

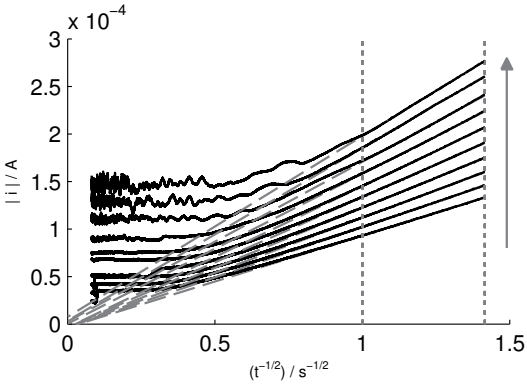

Figure 3.5. Chronoamperometric measurements of a 20 mM $FeCl_3$ solution in ethaline over a range of temperatures between 25 and 70°C in 5°C steps at the GC electrode (solid black lines indicate experimental data, which is shown to extrapolate to zero current at infinite time by dashed grey lines). The arrow indicates the direction of increasing temperature. The vertical dashed lines indicate the time interval over which fitting is performed. Publication IV

to C_{dl} flows, equation 3.12 becomes fully applicable. The point at which applicability ends is when the effect of natural convection becomes appreciable. This end point shows a reproducible and logical dependency on the temperature, since the viscosity decreases with temperature and therefore the point at which natural convection becomes significant also occurs earlier. For the sake of simplicity the lowest cut-off value, $1\mathrm{s}^{-1/2}$ at 70 °C, is used in all the fittings. The values of D determined using this method for a range of complexes and temperatures are presented in section 3.6.

3.5 Electrochemical Impedance Spectroscopy

Impedance spectroscopy is utilised across a wide range of disciplines, especially electrical engineering. In the case of highly nonlinear processes, such as the Faradaic reaction described in section 3.1, electrochemical impedance spectroscopy (EIS) proceeds from application of a small amplitude sinusoidal excitation, typically applied potentiostatically. The small amplitude, typically 10 mV, allows linearization of equation 3.6 using a Taylor series. Application of a sinusoidal excitation has three useful properties.

Firstly, equations can be more readily solved using Laplace transforms. Secondly, since the first derivative of a sine wave is also sinusoidal, the response to the excitation which is observed at the current follower is

also sinusoidal, of an identical frequency and can therefore be exactly described in terms of an impedance and phase shift. EIS measurements therefore have an outstanding resilience to noise. This property also allows the processes taking place in the system to be considered in terms of an equivalent electronic circuit. Finally, since the processes described in section 3.1 each have their own characteristic time, EIS can probe the various processes relatively independently at selected frequencies.

Traditionally, EIS measurements were performed using a lock-in amplifier, which often incorporated a sine wave generator. This was an analogue system that would register the phase angle and amplitude of the response relative to the applied signal. The next evolution was a frequency response analyser, FRA, which was traditionally a discrete instrument. An FRA performs digital integration of a sinusoidal input signal with angular frequency ω_{EIS} and the cell response, $S(t)$, to determine the real and imaginary parts of the impedance , Z_{Re} and Z_{Im}, using equations 3.13 and 3.14 [52]. An important benefit of digital integration is that the precision at lower frequencies does not diminish.

$$Z_{\mathrm{Re}} = \frac{1}{T}\int_0^T S(t)\sin\left(\omega_{\mathrm{EIS}}t\right)dt \tag{3.13}$$

$$Z_{\mathrm{Im}} = \frac{1}{T}\int_0^T S(t)\cos\left(\omega_{\mathrm{EIS}}t\right)dt \tag{3.14}$$

With a modern multifunctional DAQ, EIS measurements that allow characterization of all the relevant processes described in section 3.1 can be performed with excellent precision, at a fraction of the cost associated with commercial instruments. Manufacturers of potentiostats boast impressively high bandwidths and EIS capabilities for their instruments. But, as will be shown in section 3.5.2, unless these are combined with carefully thought out reference electrodes the result are of dubious significance. Additionally, in all the experiments carried out in this thesis no Faradaic processes were apparent at frequencies higher than 50 kHz, which is well within the range of frequencies that can be accurately synthesised by a DAQ that can output 1 MS/s (megasamples per second), such as the NI 6251 used in this work.

3.5.1 Theoretical treatment

When utilising EIS techniques it is natural to think of the various processes in the conceptual framework in terms of an electrical circuit. In

this thesis only a brief description of the parameters used and their relation to the conceptual framework will be given. For a fuller explanation the introductory text by Gabrielli is recommended [52]. All current that passes through the system must pass through the electrolyte, resulting in the solution resistance, R_{s}. In series with R_{s} are the two distinct processes due to capacitive charging of C_{dl}, and the Faradaic process taking place at the electrode respectively. In the case of the Faradaic process the electron transfer reaction is independent of frequency and also behaves as a resistor. It is referred to as the charge transfer resistance, R_{ct}, and depends on the potential in a relatively complicated manner, as shown in equation 3.15.

$$R_{\mathrm{ct}} = \frac{RT}{n^2F^2A} \cdot \frac{1}{(\alpha k_{\mathrm{f}} C_{\mathrm{O}} + (1-\alpha)k_{\mathrm{b}} C_{\mathrm{R}})} \tag{3.15}$$

Changing the electrode potential alters both the rate constants, k_{f} and k_{b}, as well as the surface concentrations C_{O} and C_{R}. The diffusive transport of the oxidized or reduced species to or from the electrode is frequency dependent and is described by what is known as a Warburg element, Z_{W}. The impedance of the Warburg element is shown in equation 3.16 and depends not only on the kinetics of the heterogeneous reaction, but also the mass transport properties and frequency.

$$Z_{\mathrm{W}} = \frac{R_{\mathrm{ct}}}{\sqrt{j\omega_{\mathrm{EIS}}}} \left(\frac{k_{\mathrm{f}}}{\sqrt{D_{\mathrm{O}}}} + \frac{k_{\mathrm{b}}}{\sqrt{D_{\mathrm{R}}}} \right) \tag{3.16}$$

Where j is the imaginary unit ($j^2 = -1$). The combination of elements described above is commonly referred to as the Randles circuit. A typical example of an experimental measurement and the result of fitting the equivalent Randles circuit is shown in figures 3.6 and 3.7.

The relationship between the impedance of a capacitor and the frequency of the applied excitation is given in equation 3.17.

$$Z_{C_{\mathrm{dl}}} = \frac{1}{j\omega_{\mathrm{EIS}} C_{\mathrm{dl}}} \tag{3.17}$$

This shows that at high frequencies the impedance of C_{dl} is zero. Therefore the measurable impedance of the system is due entirely to R_{s} and has a phase angle of 0. This situation corresponds to region 1 in figures 3.6 and 3.7. As the frequency decreases the impedance of C_{dl} becomes non-zero. Simultaneously, ω_{EIS} is still high enough that Z_{W} is essentially zero. This combination of a constant resistance and capacitor in parallel yields a semicircle in the complex plane, this is region 2 in figures 3.6 and 3.7.

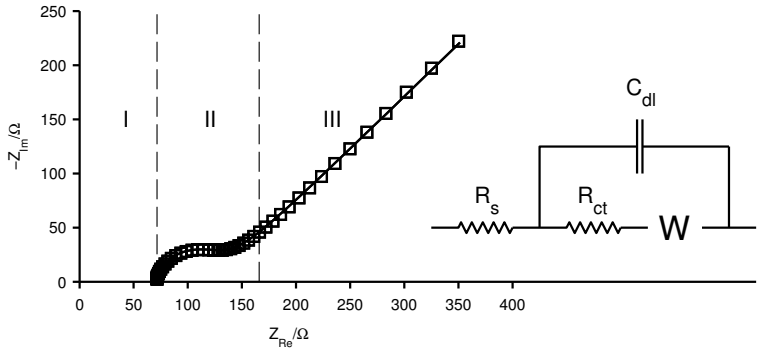

Figure 3.6. Complex plane representation of typical results for an EIS measurement in the vicinity of $E^{0'}$ for a 20 mM $CuCl_2$ solution in ethaline at 40 °C at a Pt electrode. Experimental data (❑) and fitting (-). The circuit diagram for the Randles circuit is also shown, W is the element corresponding to the Warburg impedance. Publication I

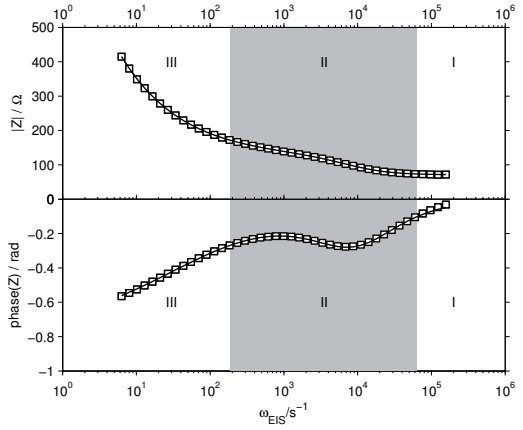

Figure 3.7. Bode plot of the data presented in 3.6, adapted from Publication I

At yet lower frequencies, the impedance of C_{dl} becomes relatively large and the majority of the current passes through the Faradaic branch of the Randles circuit. At this point the impedance of the Warburg element, Z_{W}, becomes pronounced and a straight line with an angle of 45°, corresponding to region 3, is apparent in figure 3.6.

In real electrochemical systems the capacitive process that occurs in parallel with the Faradaic process tends to show a range of time constants, this results in the phase observed being slightly less than 90°. Put another way, the tangent of the initial part of the semicircle corresponding to region 2 in figure 3.6 is not vertical. This kind of non-ideal behaviour can be described using a constant phase angle (CPE). The impedance of a

CPE is calculated using equation 3.18.

$$Z_{\mathrm{CPE}} = \frac{1}{(j\omega_{\mathrm{EIS}})^{n_{\mathrm{f}}} Y_0} \tag{3.18}$$

Where Y_0 is the standard admittance of the CPE. For a perfect capacitor the frequency exponent, n_{f}, is 1, for a perfect resistor it is 0. In this thesis the value of n_{f} observed for the CPE used to describe C_{dl} across a range of electrochemical systems was invariably close to 0.9. Since the impedance of a Warburg element, Z_{W}, depends on frequency it is useful to collect the terms which are not frequency dependent in a single parameter. Equation 3.16 then takes a form identical to that for a CPE with a n_{f} of 0.5. The standard admittance of the CPE representing the Warburg element, $Y_{0,\mathrm{W}}$, determined by fitting of the Randles circuit to experimental data can then be related to the electrochemical parameters using equation 3.16.

The only task that remains then is to estimate how the surface concentrations of the two species, C_{O} and C_{R}, depend on the electrode potential, E. For reasonably facile kinetics this can be done by rearranging the Nernst equation, shown in equation 3.19.

$$E = E^{0\prime} + \frac{RT}{nF} \ln \frac{C_{\mathrm{O,bulk}}}{C_{\mathrm{R,bulk}}} \tag{3.19}$$

The fitted values of Z_{Im} and Z_{Re} are calculated by combining equations 3.15 to 3.18 using equation 3.20.

$$Z = Z_{\mathrm{Re}} + jZ_{\mathrm{Im}} = R_{\mathrm{s}} + \left(\frac{1}{Z_{C_{\mathrm{dl}}}} + \frac{1}{R_{\mathrm{ct}} + Z_{\mathrm{W}}} \right)^{-1} \tag{3.20}$$

These are all simple analytical expressions, which are trivial to calculate. Fitting proceeds in two stages. Firstly, the individial spectra are fitted to the Randles circuit. Generally, this was achieved by using commercial fitting software (Zview 2.3d, Scribner associates) in batch fitting mode. In Publication II the fitting of spectra was performed by implementing equations 3.15 to 3.20 in matlab and performing non-linear fitting with the Levenberg-Marquardt algorithm [53].

By quantifying the dependency of R_{ct} and $Y_{0,\mathrm{W}}$ on electrode potential it is possible to demonstrate both the validity of the model as a description of the experimental system and determine all of the parameters which control the processes shown in figure 3.1. Examples of such a fitting procedure are shown in figure 3.8.

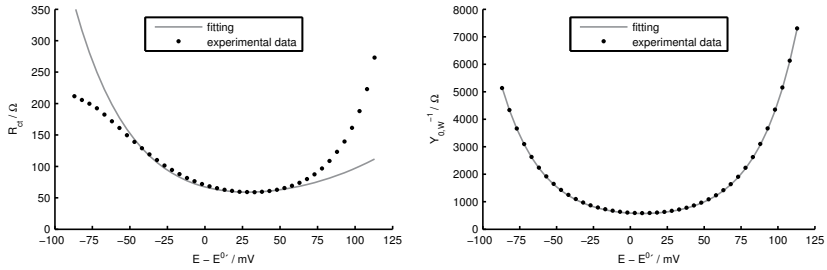

Figure 3.8. Example of determination of system parameters from R_{ct} and Z_W for a 20 mM $CuCl_2$ solution in ethaline at 40 °C on a Pt electrode. Publication I

3.5.2 Reference electrodes for EIS measurements

In Publication IV a number of separate problems that may arise from the use of a simple quasi reference electrode (QRE) were described. The obvious solution is to place the reference electrode inside a separate compartment and prevent mixing with the system under study, for instance using a vycor frit. Such a reference probe has been demonstrated by Snook et al. [54] and since it solves both the problem of contamination and reference stability has been widely recommended [19, 55].

In poorly conductive media, e.g. ionic liquids, simple calculations based on the electrolyte conductivity and frit geometry indicate that such a configuration will result in significant impedance between the reference electrode and the test solution. This is known to introduce a range of artifacts during measurements such as high speed voltammetry, potential steps or impedance spectroscopy [56, 57].

Figure 3.9 shows the effect of introducing a known resistance between the QRE and the potentiostat during impedance measurements described in Publication IV. When the added resistance is low a regular Randles circuit is observed. As the resistance of the reference electrode increases an additional semicircle appears at high frequencies. A reference electrode resistance of 10 kΩ or lower gives a result that resemble the Randles circuit reasonably well, below 2 kΩ no effect is observable.

Measurement of the reference electrode resistance, using the method described in the literature [56] resulted in values of 14 and 6000 Ω for the Pt QRE and the Ag/AgCl capillary reference probe respectively. However,

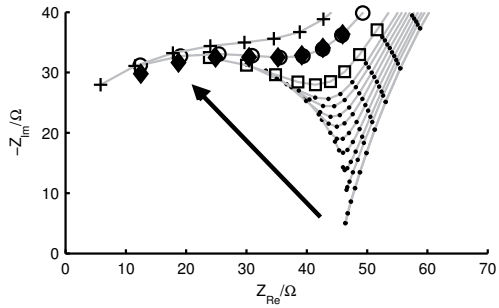

Figure 3.9. Dependency of the EIS response at frequencies between 50 and 5 kHz on the various impedances selected on the resistance box inserted between the QRE and potentiostat (•), as described in Publication IV. The arrow indicates the effect of increasing QRE impedance. Measurements performed with QRE impedance values of 50, 75 and 100 kΩ are plotted using distinct symbols (❑,○ and + respectively). Measurements performed with lower QRE impedances are not distinquished. The impedance spectrum observed when using the Ag/AgCl reference probe as the reference electrode is shown also (◆). Publication IV

as can be seen in figure 3.9, the use of the Ag/AgCl reference probe is consistent with an actual reference impedance of 75 kΩ. This would appear to indicate complications in the accurate characterisation of reference electrode performance, possibly due to additional Faradaic impedance at the Ag/AgCl surface. For a typical Vycor frit, such as that used by Snook, and an electrolyte with a conductivity of 10 mS cm^{-1} an impedance of at least 1 kΩ can be expected [58]. Such an electrode can only be reliably used in the measurement of impedance data if the properties are first characterised and shown to give similar results to parallel measurements with a QRE.

Since the majority of voltammetric techniques require accurate quantification and compensation of R_s for the accurate determination of physical parameters, these also depend on the use of a suitable reference system. Based on the work performed in the thesis, the author recommends that two reference electrodes are used, one a simple inert QRE connected to the RE terminal on the potentiostat and the other a reference probe. By regularly recording the potential between these two electrodes, using a suitably high impedance differential electrometer, the reference potential of the QRE becomes well defined. In such a configuration the dynamic characteristics and impedance of the reference probe become irrelevant.

3.6 Overview of results at a stationary electrode

The various methods outlined thus far are all applicable at a stationary electrode and it therefore makes sense to compare the consistency of these methods to quantify the properties of electrochemical processes in ILs.

3.6.1 Mass transport properties of chlorocomplexes in DES

As can be seen from figure 3.10, all three methods used to determine D work well. Since EIS involves significant complexity during the determination of D, this method is not recommended. CV is in principle a reasonable method and the most familiar to the majority of experimentalists. To achieve full accuracy it requires some care with configuration of the potentiostat, as well as validation that the sytem exhibits reversible behaviour at the scan rates used. Validation of reversible behaviour during CV measurements in an IL demands compensation of Ohmic losses and this will require at least one EIS measurement, preferably in the vicinity of $E^{0'}$.

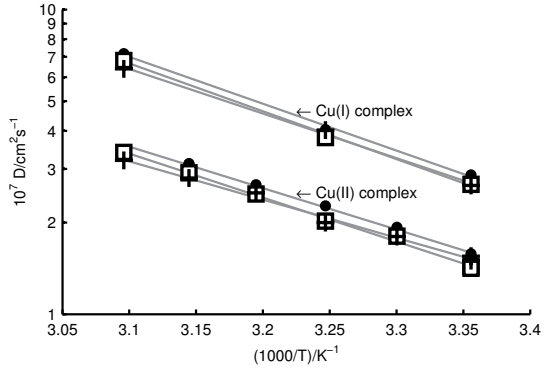

Figure 3.10. Diffusion coefficients of $[CuCl_4]^{2-}$ and $[CuCl_3]^{2-}$ in ethaline as a function of temperature (solid lines = Arrhenius fit, ● = potential step, ❑ = cyclic voltammetry, ✚ = impedance spectroscopy). Publication I

For copper the diffusion coefficient of the Cu(I) complex is twice that of the Cu(II) complex. As noted in Publication I, this pattern has been observed in other chloride based electrolyte systems and even for copper perchlorate salts in water.

The potential step method has been found to be the most reliable and simplest to apply, since it is largely unaffected by slow electrode kinetics or the effects of Ohmic losses. For this reason in Publication IV only this

method was used when determining D. The results of such a fitting are shown in figure 3.11.

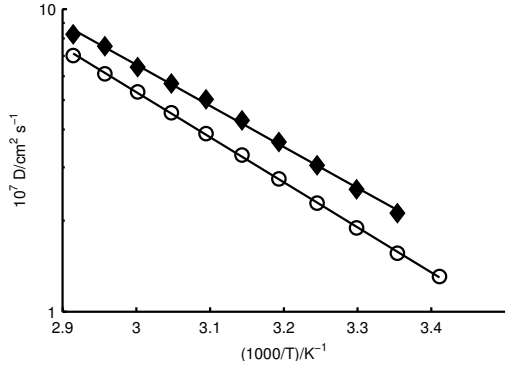

Figure 3.11. Dependency of the diffusion coefficients for $[FeCl_4]^{2-}$ (○) and $[FeCl_4]^-$ (◆) on temperature, from the fitting shown in figure 3.5. Publication IV

In a reversal of the situation in the copper system, the diffusion coefficient of the Fe(III) complex is greater than that of Fe(II). For the iron complexes this can reasonably be explained in terms of the additional negative charge on the divalent $[FeCl_4]^{2-}$ complex. The diffusion coefficient of $[FeCl_4]^-$ is four times lower in ethaline than in a chloroaluminate under similar conditions [59].

The activation energies of the diffusion coefficients are 26.0±0.9 and 28.5±0.3 kJ/mol for the trivalent $[FeCl_4]^-$ and divalent $[FeCl_4]^{2-}$ complexes respectively. These are similar to the values for $[CuCl_4]^{2-}$ and $[CuCl_3]^{2-}$, which are 27.7±1.4 and 29.5±1.5 kJ/mol respectively.

The most notable result is that the value of D for all the species examined is 40 times lower than in water, which mirrors the viscosity of the two systems closely. It was this result, in combination with the need for extensive Ohmic compensation, which first indicated to the author that technical application of DES would be challenging.

3.6.2 Electrode kinetics of chlorocomplexes in DES

As can be seen in figure 3.12, neither methods based on cyclic voltammetry nor impedance spectroscopy yield well defined values of k^0 as a function of temperature at a stationary electrode. However, as described in Publication I, the kinetic parameters determined for this system are similar to that in a range of other ILs.

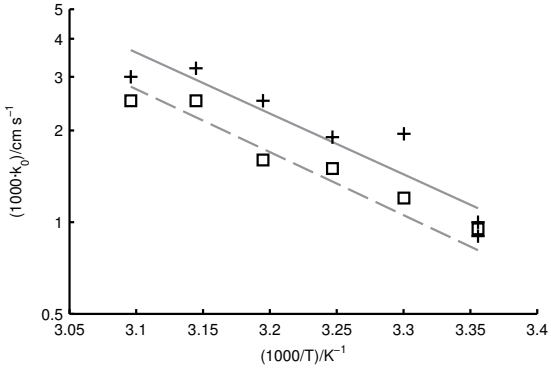

Figure 3.12. Dependency of k^0 on temperature for the Cu(I)/Cu(II) reaction at a Pt electrode in ethaline (solid line = Arrhenius fit of impedance data, dashed line = Arrhenius fit of cyclic voltammetry, ❑ = cyclic voltammetry, ✚ = impedance spectroscopy). Publication I

3.7 Rotating Disc Electrode

The greatest weakness of the experimental techniques described in the previous section was the large scatter in the values of k^0 as a function of temperature. For this reason, methods based on the use of the rotating disc electrode (RDE) were examined in Publication II as these are generally considered to provide more reliable results during electrochemical studies [60]. The RDE is the most common implementation of a class of experimental techniques based around the concept of a hydrodynamic electrode (HDE). In any kind of hydrodynamic electrode the electrolyte is no longer stationary, instead it is brought in to well defined motion.

At the RDE the electrode is a disc mounted on shaft which is rotated. The disc is sheathed in an inert material. The local effect of rotation is to accelerate electrolyte radially outwards, as in a centrifugal pump. This results in a steady stream of electrolyte being continually drawn towards the electrode surface.

This requires modification of the conceptual framework discussed in 3.1. In addition to mass transport due to diffusion, convection of electroactive species due to movement of the electrolyte must be considered. Since convection occurs in numerous directions, this requires a change in notation and addition of a convection term to equation 3.1, this yields equation 3.21.

$$\vec{N_{\mathrm{R}}} = -D_{\mathrm{R}}\nabla C_{\mathrm{R}} + \vec{v}C_{\mathrm{R}} \tag{3.21}$$

In the discussion that follows the hydrodynamics are only considered for systems exhibiting laminar flow. This not only simplifies the theoretical treatment, it also reflects the reality that experimental results collected at an electrode exhibiting turbulent flow are noisy and therefore poorly defined. It also assumes a Newtonian fluid. Generally speaking, the velocity profile of the electrolyte in front of the electrode would be expected to show a complex spatial dependency. Remarkably, for the RDE the effect of convection shows radial uniformity, i.e. the convective velocity only depends on the distance from the electrode surface, x. A hydrodynamic system that exhibits this behaviour is described as being uniformly accessible and benefits from a simplified theoretical treatment. In the vicinity of the surface of the RDE the axial velocity of the electrolyte has been

shown to be well described by equation 3.22 [61].

$$v_{\mathrm{x}} = -0.51\omega_{\mathrm{RDE}}^{3/2}\nu^{-1/2}x^2 \tag{3.22}$$

Where ω_{RDE} is the angular frequency of the RDE and ν is the kinematic viscosity, which is related to the dynamic viscosity, η, by equation 3.23, where ρ is the density of the electrolyte.

$$\nu = \eta/\rho \tag{3.23}$$

Close to the electrode surface v_{x} is 0 and therefore mass transport is entirely due to diffusion, as x increases the role of convection rapidly increases. This means that the system can readily reach a well defined steady state where a constant flux of electroactive species to and from the electrode is observed. Theoretical treatment of combined convective and diffusive transport is almost invariably based on a simplified model which assumes a distinct value of x up to which the mass transport is entirely due to diffusion and beyond which convection is so rapid that the concentration is constant and equal to bulk conditions. This is the Nernst diffuse layer model and the point at which this transition occurs is referred to as the Nernst layer thickness, δ. The thickness of the Nernst layer depends on a number of parameters, as shown in equation 3.24.

$$\delta = 1.61D^{1/3}\omega_{\mathrm{RDE}}^{-1/2}\nu^{1/6} \tag{3.24}$$

An example of simulated concentration profiles during a potential sweep at the RDE are shown in 3.13. These show that the approximation is accurate in the immediate vicinity of the electrode and the extrapolated tangents of the fluxes at $x = 0$ pass through a single point, corresponding to $x = \delta$.

For a system where the diffusion coefficient of the oxidised and reduced species, D_{O} and D_{R}, are different equation 3.24 results in the slightly counter-intuitive result that $\delta_{\mathrm{R}} \neq \delta_{\mathrm{O}}$. The important simplification that the RDE gives is that when a constant potential is applied for sufficient time, typically a few seconds, the system will reach a steady-state and the fluxes between the electrode and bulk phases can be described using a simplified form of equation 3.1, as shown in equation 3.25.

$$N_{\mathrm{R}} = -D_{\mathrm{R}}\frac{(C_{\mathrm{R,bulk}} - C_{\mathrm{R}}|_{x=0})}{\delta_{\mathrm{R}}} \tag{3.25}$$

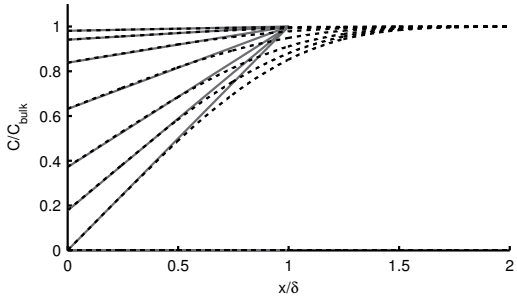

Figure 3.13. Simulated concentration profiles during a slow potential sweep at the RDE. Simulated concentration profiles (dashed lines); tangent of the concentration profile at $x = 0$ (solid lines). Adapted from original data prepared by T. Vainikka [51]

3.7.1 Voltammetry at the RDE

The theory above forms the basis for the electrochemical technique traditionally used with the RDE. In this method the electrode is rotated at a constant angular frequency and the potential is slowly swept, as in cyclic voltammetry. When the scan-rate is sufficiently slow, the system is in a state of continuous quasi-equilibrium, with linear concentration profiles across the Nernst layer, hence equation 3.25 applies. A typical example of a series of such sweeps is shown in figure 3.14.

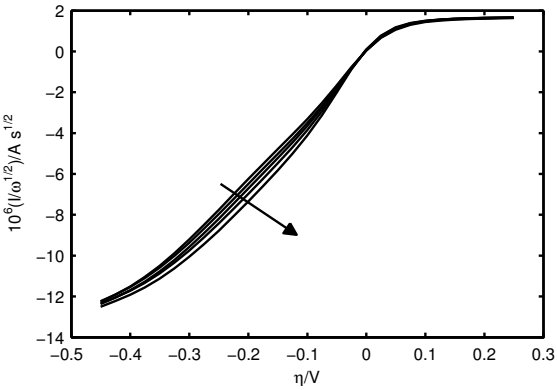

Figure 3.14. Normalised staircase voltammetry data for a 20 mM $CuCl_2$ electrolyte at a 5mm GC electrode at rotation rates of 1000, 1250, 1500, 1750 and 2000 rpm. The arrow indicates decreasing rotation speed. 100% IR correction was applied during acquisition of the voltammogram. Publication III

As can be seen from equation 3.6, when the current is zero then the rate of the forward and back reactions must be equal, the system is in equilibrium and the concentration profiles are flat. Hence, this potential

is defined as the equilibrium potential, E_{eq}, and is given by the Nernst equation (3.26).

$$E_{\text{eq}} = E^{0'} + \frac{RT}{nF} \ln \frac{C_{\text{O,bulk}}}{C_{\text{R,bulk}}} \tag{3.26}$$

This allows the potential scale to be normalised around a single experimentally observable point where the reactions are in equilibrium. This provides the definition of overpotential, η, given in equation 3.27.

$$\eta = E - E_{\text{eq}} \tag{3.27}$$

At large cathodic or anodic overpotentials the characteristics of the electrode reaction are dominated by either k_{f} or k_{b} respectively, since the other rate constant is effectively zero. At particularly large overpotentials the kinetics cease to measurably depend on overpotential and the surface concentration of the reacting species drops to zero. Increasing the overpotential will no longer result in an increase in current as the system is fully mass transport limited. The plateau current observable is known as the limiting current, I_{l}. Equations for the anodic and cathodic limiting currents, $I_{\text{l,a}}$ and $I_{\text{l,c}}$ respectively, are given in equations 3.29 and 3.28, which are both forms of the Levich equation.

$$I_{\text{l,c}} = \frac{-nFAD_{\text{O}}C_{\text{O,bulk}}}{\delta_{\text{O}}} \tag{3.28}$$

$$I_{\text{l,a}} = \frac{nFAD_{\text{R}}C_{\text{R,bulk}}}{\delta_{\text{R}}} \tag{3.29}$$

Part of the improvement in precision gained by using the RDE is simply due to the ability to combine knowledge of the diffusion coefficients with measurements to determine the limiting currents. This provides a simple means to accurately quantify the drift in bulk concentrations as a series of experiments proceed.

At slightly lower overpotentials one of the rate constants will still show some dependency on potential. It is then interesting to imagine what would happen if the rate of rotation could be increased to infinity, without the transition from laminar to turbulent flow occuring. In such a case the Nernst layer thickness would become zero, no mass transport limitations would exist and the surface concentrations would be equal to the bulk concentrations. The current that would then be observable would be a purely kinetically controlled current, I_{K}, and is defined in equations 3.30 and 3.31 for substantial cathodic or anodic overpotentials respectively.

$$I_{\mathrm{K,c}} = -FAk_{\mathrm{f}}C_{\mathrm{O,bulk}} \tag{3.30}$$

$$I_{\mathrm{K,a}} = FAk_{\mathrm{b}}C_{\mathrm{R,bulk}} \tag{3.31}$$

In such a situation, equations 3.25 and 3.6 can be combined with equations 3.28-3.31 and simplified to give what is known as the Koutecký-Levich equation, which is shown in equation 3.32.

$$\frac{1}{I} = \frac{1}{I_{\mathrm{K}}} + \frac{1}{I_{\mathrm{l}}} \tag{3.32}$$

Since I_{K} does not depend on ω_{RDE}, but I_{l} shows a linear relation dependency on $\omega_{\mathrm{RDE}}^{1/2}$, this means that plotting $1/I$ as a function of $\omega_{\mathrm{RDE}}^{-1/2}$ will, for suitable overpotentials, yield a straight line with a constant slope and an intercept with the ordinate-axis equal to $1/I_{\mathrm{K}}$. This provides a simple means to take data collected over a range of finite ω_{RDE} values and extrapolate to determine the behaviour of the system when $\omega_{\mathrm{RDE}} = \infty$. Such a plot is known as a Koutecký-Levich plot. An example of which is given in figure 3.15.

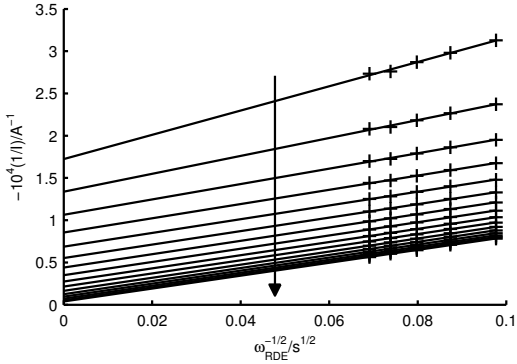

Figure 3.15. Koutecký-Levich plots prepared from the voltammetric data shown in figure 3.14 for η values between -0.05 and -0.4 V. The arrow indicates increasingly negative overpotentials. Publication III

When the logarithm of $|I_{\mathrm{K}}|$ is plotted as a function of overpotential the result is what is known as the Tafel plot, an example of which is shown in figure 3.16.

At sufficiently large overpotentials $\log(|I_{\mathrm{K}}|)$ shows a linear dependency. From equations 3.4 and 3.5 it is clear that the slopes of the cathodic and anodic branches in the Tafel plot are $-\alpha f$ and $(1-\alpha)f$ respectively. Either of the two linear branches of the Tafel plot can be extrapolated to zero

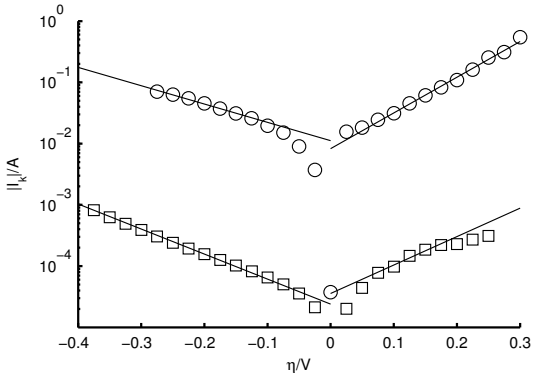

Figure 3.16. Tafel plot for a 20 mM $CuCl_2$ electrolyte at a glassy carbon electrode (❑) and a 2 M CuCl electrolyte at a graphite electrode (❍) The I_K values for the GC electrode measured at negative η values are determined from the intercept of the Koutecký-Levich plots shown in figure 3.15. Publication III

overpotential to yield what is known as the exchange current, I_0. Since η is 0, equations 3.30 or 3.31 can be combined with equations 3.5 or 3.4 respectively to determine k^0, as shown in equations 3.33 and 3.34.

$$I_{0,c} = FAk^0 C_{0,bulk} \tag{3.33}$$

$$I_{0,a} = FAk^0 C_{R,bulk} \tag{3.34}$$

In the predigital era, a family of steady-state voltammograms could be collected for different values of ω_{RDE} on a single piece of paper using an x-y plotter. The current at a range of rotation speeds and overpotentials could be readily transferred to a Koutecký-levich plot and manually extrapolated to give I_K. This in turn could be transferred to semilog graph paper to prepare a Tafel plot, from which α and k^0 could be determined. Such a technique involves a minimum of computation and would clearly be strongly favoured in a time before the wide spread availability of personal computers.

This method is primarily limited by the accuracy of the extrapolation process. In addition to random noise, the current-potential function observed during a series of measurements will be affected by some drift in the bulk concentrations, which affects both $I_{l,c}$ and $I_{l,a}$. This problem becomes most pronounced at larger overpotentials, since the intercept of $1/I$ approaches zero and even a relatively small extrapolation error will become rather pronounced when the reciprocal is taken to determine I_K.

3.7.2 EIS at the RDE

In section 3.5.1 the dependency of the surface concentration on the potential was assumed to be described adequately by the Nernst model. While this assumption may be reasonably valid, its application depends on knowledge of both species bulk concentrations, which can be problematic. By constrast, in section 3.7.1 it was shown that for voltammetric techniques at the RDE it was possible to perform a nearly complete analysis of the kinetics of the system without detailed knowledge of the transport properties.

While the use of the RDE as a tool during EIS measurements is commonly recommended, the author could not find a concise explanation of a suitable experimental procedure and theoretical treatment. Hence in Publication II the relevant theory was lain out and tested for the same electrochemical system studied in Publication I. The experiment is performed by stepping DC potential, waiting a short period for the current to stabilise, performing an EIS measurement, sampling the DC current and then moving to the next DC potential. The experiment is designed to span a sufficiently wide range of potentials that both limiting currents are observed, however there is no requirement that the potentials selected are homogeneously distributed within that range. It is better to concentrate on potentials where R_{ct} is relatively small as this is where EIS is most sensitive to the Faradaic process.

Analysis of the experimental data proceeds as follows. Firstly, the observables $I_{\mathrm{l,c}}$ and $I_{\mathrm{l,a}}$ can be used to estimate the bulk concentrations of both species by combining equations 3.29 and 3.28, as shown in equation 3.35.

$$\frac{C_{\mathrm{O,bulk}}}{C_{\mathrm{R,bulk}}} = \frac{-I_{\mathrm{l,c}}}{I_{\mathrm{l,a}}} \left(\frac{D_{\mathrm{R}}}{D_{\mathrm{O}}} \right)^{2/3} \tag{3.35}$$

Since the total bulk concentration of both species is unlikely to change significantly during a measurement, this reduces one source of uncertainty. Once $C_{\mathrm{O,bulk}}/C_{\mathrm{R,bulk}}$ is known, a good initial estimate of $E^{0'}$ can be made from the observable E_{eq} using equation 3.26. The provision of initial estimates based on observable properties of the system both improves the ease of fitting and provides a means to validate the process, since the difference between initial and fitted values should be small.

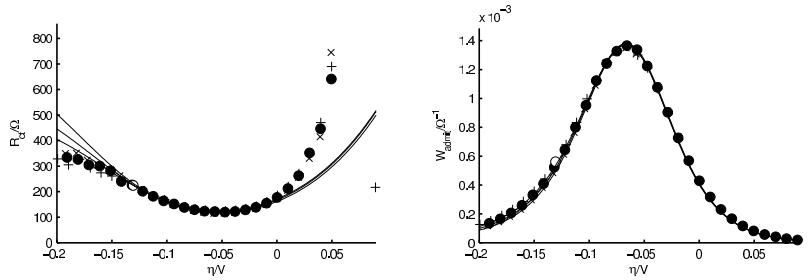

Figure 3.17. Dependency of R_{ct} and $Y_{0,\mathrm{W}}$ on overpotential for three rotation speeds measured at 30 °C: 2500 (+), 2000 (●) and 1500 (×) RPM; fits (—); Publication II

Most importantly, equations 3.25 and 3.35 can be combined to provide estimates of the potential depend surface concentrations C_{O} and C_{R} from the observables, I, $I_{\mathrm{l,a}}$ and $I_{\mathrm{l,c}}$, as shown in equations 3.36 and 3.36.

$$C_{\mathrm{O}}|_{x=0} = C_{\mathrm{O,bulk}} \left(1 - \frac{I}{I_{\mathrm{l,c}}}\right) \tag{3.36}$$

$$C_{\mathrm{R}}|_{x=0} = C_{\mathrm{R,bulk}} \left(1 - \frac{I}{I_{\mathrm{l,a}}}\right) \tag{3.37}$$

Since the DC current, I, in an RDE experiment is non-zero, except at E_{eq}, and the solution resistance, R_{s}, is known precisely, it is trivial to perform complete post-experimental correction of the steady-state voltammetric data by calculating the actual electrode potential, E, from the observable electrode potential, E_{obs}, as shown in equation 3.38, which is simply Ohm's law.

$$E = E_{\mathrm{obs}} - IR_{\mathrm{s}} \tag{3.38}$$

The rest of the fitting process is essentially the same as that described in section 3.5.1. Use of the RDE during EIS measurements, in combination with the techniques described in this section, provides both a simple and robust method to determine a wide range of system properties. Examples of such a fitting for the $[CuCl_4]^{2-}$ complex are shown in figure 3.17.

Figure 3.17 shows that the rate of rotation has no discernible effect on the EIS results and, in principle, it is sufficent to study the system at one value of ω_{RDE}, provided the mechanism is well understood. The resulting k^0 values for the Cu(I)/Cu(II) redox reaction are shown in figure 3.18, with

those determined at the stationary electrode also shown for reference.

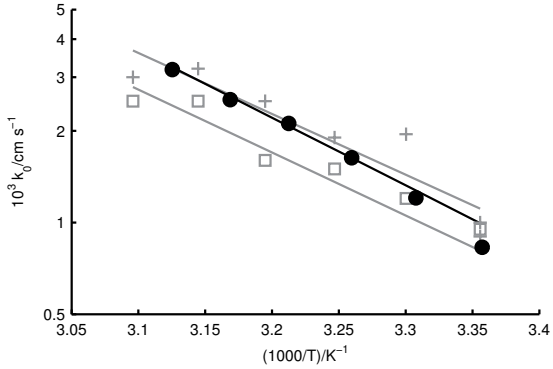

Figure 3.18. Arrhenius plot of the standard rate constant, k^0, from EIS measurements at a Pt RDE (●), results for a stationary electrode, previously shown in figure 3.12, are also included for reference (+,❑). Adapted from publications I and II

As is clear from figure 3.18, the estimate of k^0 from EIS at an RDE shows a more even distribution as a function of temperature, which suggests the technique is less error prone than EIS measurements at a stationary electrode. However, the stationary electrode certainly provides a reasonable indication of the system properties. The value of k^0 determined for the Cu(I)/Cu(II) reaction at a GC electrode in Publication III was 20 times lower than the values for the Pt electrode shown in figure 3.18.

A final attractive aspect of performing EIS at the RDE is that when the angular frequency of the AC excitation, ω_{EIS}, is sufficiently low the technique is sensitive to the Nernst layer thickness. This requires replacement of the Warburg element used in section 3.5.1 with a short-circuit Warburg element, the impedance of which is given by equation 3.39.

$$Z_{\mathrm{W,s}} = \frac{R_{\mathrm{ct}}}{\sqrt{j\omega_{\mathrm{EIS}}}} \left(\frac{k_{\mathrm{f}} \cdot \tanh(\delta_{\mathrm{O}} \sqrt{j\omega_{\mathrm{EIS}}/D_{\mathrm{O}}})}{\sqrt{D_{\mathrm{O}}}} + \frac{k_{\mathrm{b}} \cdot \tanh(\delta_{\mathrm{R}} \sqrt{j\omega_{\mathrm{EIS}}/D_{\mathrm{R}}})}{\sqrt{D_{\mathrm{R}}}} \right) \tag{3.39}$$

Figure 3.19 shows a typical example of this dependency. As can be seen, the effect of increasing the rotation frequency of the RDE is to compress the Nernst layer, leading to development of a second semicircle which terminates at the Z_{Re} axis.

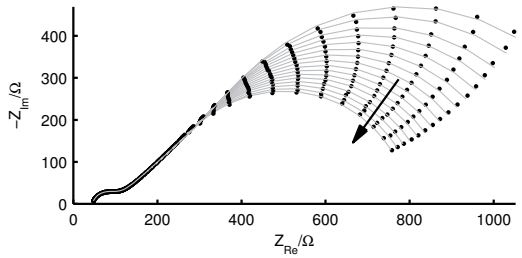

Figure 3.19. Impedance spectra measured at different rotation speeds at 50 °C and η = 110 mV (●) and fits to Randles' circuit (—); the arrow indicates increasing rotation speed

Such a technique can be useful if the thickness of the Nernst layer requires quantification and was applied in publication IV.

3.8 Viscosity and conductivity measurements

As shown in section 3.7 the kinematic viscosity of the electrolyte, ν manifests itself in electrochemical measurements at a HDE. This can be used to determine the Stokes' radii of the diffusing species with high precision, since measurements to determine both D and η can be performed concurrently under identical conditions.

As shown in equation 3.7 the conductivity of the electrolyte, κ, is also apparent from the solution resistance, R_{s}, observed during EIS measurements. Figure 3.20 shows the Arrhenius plot for the fluidity and molar conductivity values determined using both direct rheometric or conductivity measurements and based on electrochemical techniques.

The activation energies for the dynamic viscosity are 28.4±0.7 and 27.7±0.4 kJ/mol, for the rheometer and RDE measurements, respectively. These values correlate well with the activation energies of the electrolyte conductivity measured directly and estimated from the value of R_s determined in the EIS measurements (24.8±0.7 and 28.2±0.4 kJ/mol, respectively) and the activation energies of the diffusion coefficients reported in 3.6. This is entirely expected for an ionic liquid exhibiting normal behaviour, as shown later in the Walden plot.

The relatively close agreement between the electrochemical and tradi-

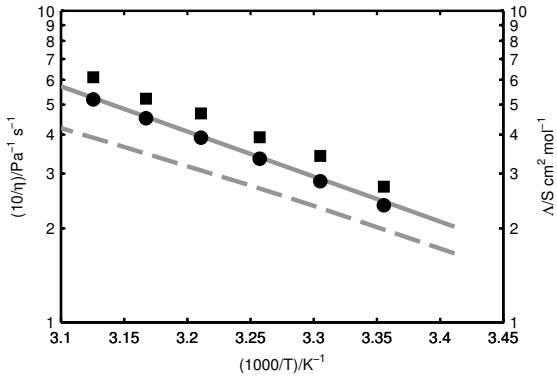

Figure 3.20. Arrhenius plot of electrolyte fluidity (reciprocal dynamic viscosity) and molar conductivity: fluidity using RDE (■); molar conductivity from EIS (●); rheometric measurements (—); AC conductivity measurements (– –). Publication II

tional techniques used to quantify viscosity and conductivity shows that electrochemical experiments can provide a reasonable indication of these two key properties of ILs, certainly with sufficient precision to allow a decision to be made whether the IL is sufficiently interesting to warrant more precise measurements.

Figure 3.21 locates the conductivity and fluidity data for ethaline in a Walden plot that also includes a selection of accepted ionic liquids. The similar activation energies for conductivity and fluidity reported above already indicate that the Walden representation of the results for ethaline should be parallel to the so-called 'ideal line' associated with dilute KCl solutions. This is considered to be indicative of ordinary ionic conduction, with an absence of electronic or Grotthus ionic conduction.

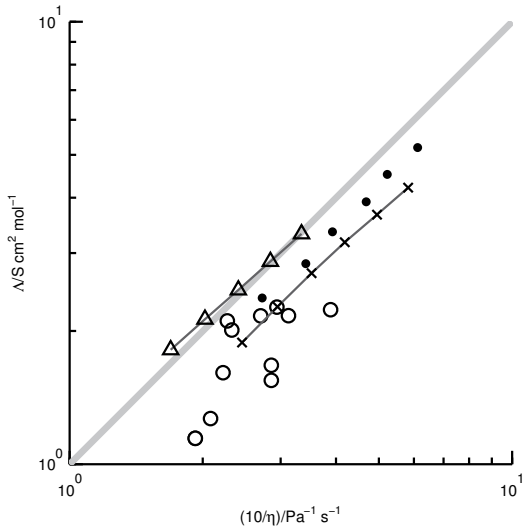

Figure 3.21. Walden plot of the correlation between conductivity and fluidity: rheometric and conductivity measurements of ethaline (×); estimates of conductivity and viscosity from RDE measurements of ethaline (●); ethylammonium nitrate [17] (△); imidazolium cations with TFSI anion [18] (○); dilute aqueous KCl solutions (grey line). Publication II

The data for ethaline is rather close to the 'ideal line' and located favourably relative to many of the imidazolium based ILs, which shows that it has transport properties analogous to those of an ionic liquid. Similar activation energies for both fluidity and molar conductivity also provide evidence which tentatively suggests that choline chloride is fully dissociated in this DES.

3.9 Wall-jet electrode

The acquisition of a commercial RDE is a non-trivial expense. This reflects the precision required during manufacturing of the electrodes, rotator and shaft if the centre of mass and the axis of rotation are to be aligned. This is an important prerequisite for the correct functioning of a RDE [62]. This also places limits on the ease with which a wide range of substrates can be tested in a RDE.

An alternative HDE is the wall-jet electrode (WJE). In this system the electrolyte is brought in to motion using either a pump [63] or pressurization [64]. The electrolyte is directed through a nozzle to the electrode

surface. By separating the convective system and electrode the demands placed on electrode construction are relaxed. The biggest drawback to the WJE is the accuracy of available methods to quantify flow.

When the system is dimensioned so that the nozzle radius, r_{T}, is larger than both the electrode radius and the nozzle-electrode separation, a major simplification in the equations describing the system behavior results. The thickness of the Nernst layer, δ, becomes uniform over the entire electrode surface and the mass transport properties of the system can therefore be accurately described by a one dimensional model, as is the case for the RDE. The electrode also becomes uniformly accessible. This configuration of the WJE is referred to as a wall-tube electrode (WTE). In any other nozzle-electrode configuration this simplification is not applicable and a two dimensional model based on cylindrical coordinates is the minimum requirement. This distinction is important not only for a simplified theoretical treatment. The WTE configuration also eliminates the tight constraints on both electrode symmetry and alignment in the electrolyte flow, thereby simplifying operation and manufacturing of the system.

The three requirements for a functional WTE are laminar flow conditions, that the surface of the electrode be flat and the electrode located directly in front of and equidistant from the nozzle opening [64]. If these requirements are met then the same techniques described in section 3.7.2 can be applied [65]. Albery and Bruckenstein have shown that the only modification is to the equation describing δ, where ω_{RDE} can be replaced by the expression given in equation 3.40 [66].

$$\omega_{\mathrm{RDE}} = \frac{V_{\mathrm{f}}}{r_{\mathrm{T}}^3} \tag{3.40}$$

This can be combined with equation 3.24 to yield an estimate for δ based on the nozzle aperature, r_{T}, and electrolyte flow rate, V_{f}, as shown in equation 3.41.

$$\delta = 1.61 D^{1/3} \frac{r_{\mathrm{T}}^{3/2}}{V_{\mathrm{f}}^{1/2}} \nu^{1/6} \tag{3.41}$$

3.9.1 Preparation of WTE system

The WTE system was based around a heavily modified square polycarbonate flask connected to a centrifugal pump. The outlet from the pump

was passed through a thermostatted glass spiral to maintain temperature control. After the spiral the outlet stream was split, with one branch passing through a flow meter (Swissflow SF800) to a hose tail attached to the centre of the flask bottom, this is the WTE feed. The other branch passes directly to the flask side, this is the bypass feed. By pinching either of the two feed tubes the flow to the WTE is regulated, while still maintaining steady flow through the pump and spiral

The WTE itself was machined from Teflon and attached to the bottom of the flask. The inner and outer diameters of the nozzle were 14 and 50mm respectively. The separation between the nozzle and electrode was 8mm. The electrode was a 5mm GC disc embedded in a Teflon disc of equal outer diameter to that of the nozzle. The surface of the electrode was coplanar with the Teflon disc and maintained at both a well-defined separation from the nozzle and in a centred alignment by three nylon screws passing through the disc and the rim of the nozzle.

A counter electrode was prepared from a loop of tungsten wire. This loop followed the lower edge of the rim of the nozzle, a position intended to ensure a homogeneous current distribution over the opening between the nozzle and the electrode. A Pt wire QRE was used and found to give 0 V of potential difference to the tungsten counter electrode when the cell was open circuit, indicating that tungsten is inert. All the electrodes and the temperature probe were passed through a polycarbonate lid resting on the edge formed where the top of the flask had been removed.

Pumping of the electrolyte was achieved using a high pressure, magnetically coupled centrifugal pump (Iwaki, MD-30RZ). The heat developed by the pump during operation was substantial and in the absence of cooling using the glass spiral resulted in a steady-state operating temperature of around 80 °C. For this reason adjustment of the WTE system temperature was slow and imprecise and detailed experiments were only attempted at one temperature.

3.9.2 Correlation of current and hydrodynamics

Figure 3.22 shows the results of measurements to quantify the linearity of the relation between volumetric flow and limiting cathodic current. In the case of the optical flow transducer the correlation is poor, with an R^2

of only 0.9629 and a non-zero intercept, this is inferior to the results reported by Rees et al.[64] as well as the specifications of the transducer. The lower sensitivity limit of the flow transducer in the standard configuration is also problematic, with no flow measurable below 0.5 dm^3 min^{-1}, the upper sensitivity limit for the flow transducer is not achievable due to the onset of turbulent flow in front of the GC disc, which manifests itself as a sudden leap in limiting current, as apparent in figure 3.22. Under turbulent conditions the limiting current becomes very poorly defined and shows significant noise. EIS measurements are also error prone under turbulent conditions.

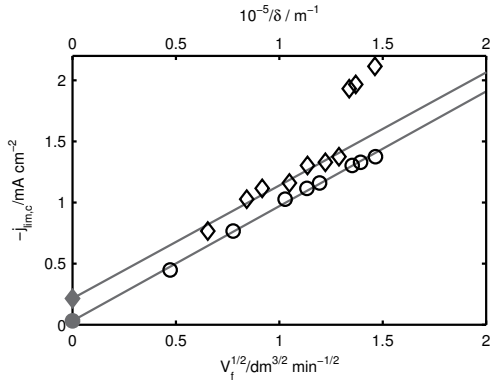

Figure 3.22. Correlation between $j_{l,c}$ and the parameters characterising the inverse Nernst layer thickness: $1/\delta$ for the EIS measurements (○) and $V_{\mathrm{f}}^{1/2}$ for the flow transducer (◊). The lines indicate the least squares fit through the experimental data for the laminar flow regime. The intercept with the ordinate axis is indicated for both the flow transducer (◆)and EIS measurements (●). Publication IV

To validate that the problem was due to the flow transducer precision, EIS measurements were performed at each flow rate to a lower frequency of 0.2 Hz, at which point the second semicircle in the complex plane plot is well developed and the parameters describing the short circuit Warburg impedance can be determined using equation 3.39. These yield a direct estimate for δ. This shows an improved correlation with the limiting dc current, with a R^2 of 0.9953. At large cathodic overpotentials the linearity of the Koutecký-Levich plots for the RDE are excellent, with a R^2 value greater than 0.9999. This is significantly superior to the values reported here and by Rees et al.[64] for the WTE and reflects the exceptionally precise and reproducible control of convection that is attainable with a commercial RDE.

3.9.3 Application of EIS at the WTE

Since the accuracy of the traditional DC methods depends upon the precision with which flow can be quantified the prospects of applying these for the WTE system described in this thesis were extremely poor. However, as shown in figure 3.17 the results for EIS measurements at a uniformly accessible electrode do not depend strongly on δ, provided it is constant for the duration of the experiment. Figure 3.23 shows the experimental and fitted values of the charge transfer impedance, R_{ct}, for measurements performed at the RDE and WTE under essentially identical conditions.

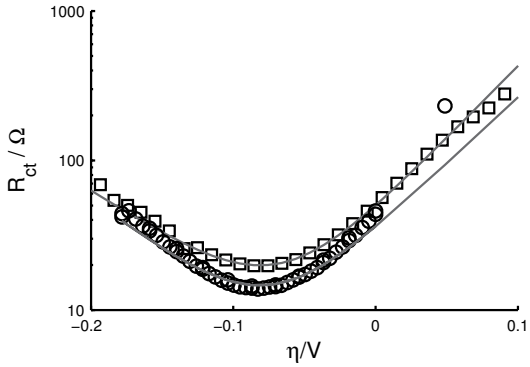

Figure 3.23. Measured values of R_{ct} as a function of overpotential for the WTE (❍) and RDE (❑) for a 20 mM $FeCl_3$ electrolyte. The lines show the fitted values. Publication IV

A difference is discernible and results in a k^0 for the WTE that is equivalent to that measured at the RDE when the temperature is 5 °C higher. However, the agreement between experiment and model is good over a wide range of potentials, which suggests that the difference may be attributable to differences in electrode preparation or aging of the electrolyte. Figure 3.24 shows the temperature dependency of k^0, calculated directly from the R_{ct} values, for the RDE and WTE.

The activation energy for k^0, E_{a,k^0}, is 45.6±0.6 kJ/mol for the Fe(II)/Fe(III) reaction at a GC electrode. This is significantly higher than for charge or mass transport and indicates that at higher temperatures the observed redox process is strongly dominated by mass transport limitations. The kinetics of the Fe(II)/Fe(III) reaction are around 40 times faster than the Cu(I)/Cu(II) reaction on GC electrodes and even exceed the rate rate of the Cu(I)/Cu(II) reaction on Pt.

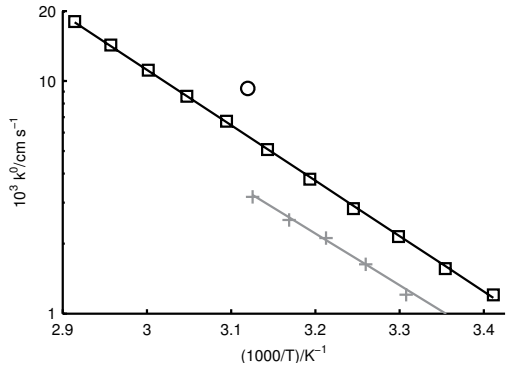

Figure 3.24. Dependency of k^0 for the Fe(II)/Fe(III) reaction on temperature for a GC RDE (❑) and GC WTE (○). The values determined for the Cu(I)/Cu(II) reaction using the a Pt RDE are shown for comparison (+). Publication IV

The standard admittance of the Warburg element, shown in figure 3.25, is virtually identical for both hydrodynamic electrodes and conforms well to theory over the range of potentials measured.

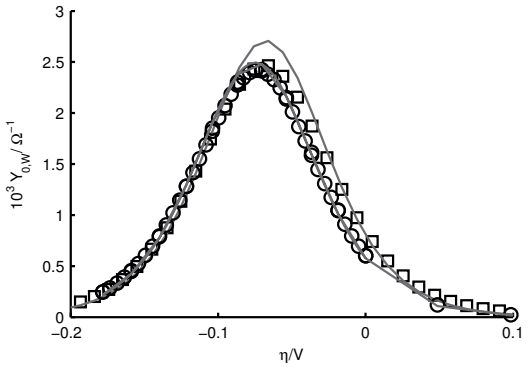

Figure 3.25. Measured values of the standard admittance of the Warburg element as a function of overpotential for the GC WTE (○) and GC RDE (❑) for the Fe(II)/Fe(III) reaction. The lines show the fitted values of the admittance. Publication IV

At higher temperatures the diffusion coefficients determined from fitting of the Warburg impedance do differ by 20% from those determined by the potential step method. An inevitable problem when determining diffusion coefficients from impedance data is that the process is dependent on simultaneous characterisation of the heterogeneous kinetics and therefore sensitive to any errors in that fitting process.

Figure 3.26 shows the excellent agreement between the observed voltammetric response at the WTE and RDE and the response predicted by parameters determined from EIS fitting. This demonstrates the accuracy of the fitting methodology, the suitability of the quasireversible mechanism and the equivalence of the RDE and WTE. At higher temperatures, e.g. 50 °C, the voltammetric response is essentially reversible and indicates that reaction 4.4 is facile.

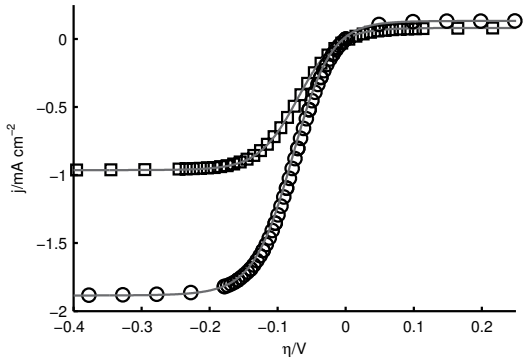

Figure 3.26. Measured voltammograms for the Fe(II)/Fe(III) reaction at the GC RDE (❑) and GC WTE (❍). The lines shows the estimated voltammograms based on the results of fitting of EIS results. Publication IV

4. Redox Flow Batteries based on deep eutectic solvents

4.1 Introduction

In recent times battery technology has been primarily applied at a small scale in a mobile setting. Even when applied in a stationary setting, such as an uninterruptible power supply (UPS), the overriding design constraint is zero maintenance, i.e. when the battery stops working it is replaced. This demands a simple, safe, closed system.

The redox flow battery (RFB) represents a radical departure from this paradigm. An example of a RFB is shown in figure 4.1. The electroactive species are dissolved in two electrolytes which are pumped through a cell where they react at two electrodes which are separated by some kind of membrane. The energy and power capacity of an RFB are decoupled, since these two properties now depend on the size of the electrolyte storage tanks and cell respectively. An open, modular system like this is more reminiscent of an electrosynthesis or electrorefining process and particularly a fuel cell.

Such a system is always more complex than a typical battery. Therefore, balance of plant costs and maintenance requirements lead automatically to relatively large scale applications. The low energy density, long life and good scaling characteristics lead to the major application as stationary energy storage devices for balancing of grids. This explains the high level of interest in the United States, which reflects the problems experienced there in achieving continual stable operation of all parts of the grid. In Europe, particular impetus has also been recently given by the planned massive increase in renewable electricity production. The nom-

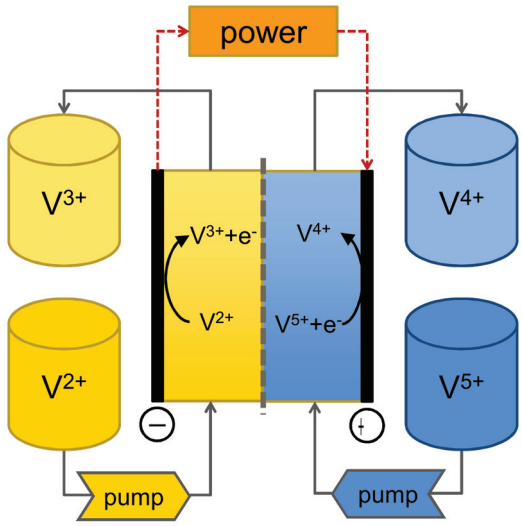

Figure 4.1. Diagram of a typical all-vanadium RFB

inal availability of a single intermittant renewable source decreases as its localised market penetration increases [67]. Hence, it is useful to have an energy storage system to ensure supply and demand are well balanced.

The intended level of renewable energy production is vast compared to the current situation. A clear example is the 2020 vision of the European Union, which intends to achieve a doubling of renewable electricity production in the EU between 2010 and 2020, largely by trebling the output of intermittant renewable sources, such a wind and solar energy [68]. This potentially represents a unique opportunity for RFBs to enable a major improvement in the sustainability of electricity production by allowing these projects are to achieve their full potential of entirely replacing an equivalent amount of fossil-based generation capacity.

4.2 Basic electrochemical research targeted at RFB applications

Only a small number of transition metals are currently produced at a sufficient scale to be suitable for application in the storage of a meaningful fraction of global daily electricity production, for instance iron, aluminium, copper and zinc [16]. When the competing economic functions these elements may perform are taken in to account then the list of plausible elements becomes very short indeed if RFB technology is to achieve

its full potential as a key enabler of large scale sustainable energy production.

Since copper is one of the most widely produced metals and was already familiar from the work performed in publications I and II, it was obvious to examine an all-copper RFB. This was the work undertaken in publication III. The all-copper redox battery has been studied by Porterfield and Yoke for the chlorocuprate ionic liquids they investigated in the seventies [69]. Kratochvil and Betty also reported a redox battery based on copper perchlorate salts dissolved in acetonitrile and reported Coulombic efficiencies close to 100% [70]. The reactions in a redox battery based on chlorocuprates are shown in equations 4.1 and 4.2.

$$\text{Negative electrode: } [CuCl_3]^{2-} + e^- \underset{\text{discharge}}{\overset{\text{charge}}{\rightleftharpoons}} Cu + 3\,Cl^- \tag{4.1}$$

$$\text{Positive electrode: } [CuCl_4]^{2-} + e^- \underset{\text{charge}}{\overset{\text{discharge}}{\rightleftharpoons}} [CuCl_3]^{2-} + Cl^- \tag{4.2}$$

In this thesis the application of deep eutectic solvents (DES) as the electrolyte media for an all-iron redox flow battery (RFB) based on the chlorocomplexes of iron was also investigated. The all-iron RFB was first studied by Hruska and Savinell [71] in a hydrochloric acid based electrolyte. In a chloride based all-iron RFB the two electrode reactions are as shown in equations 4.3 and 4.4.

$$\text{Negative electrode: } [FeCl_4]^{2-} + 2\,e^- \underset{\text{discharge}}{\overset{\text{charge}}{\rightleftharpoons}} Fe + 4\,Cl^- \tag{4.3}$$

$$\text{Positive electrode: } [FeCl_4]^{-} + e^- \underset{\text{charge}}{\overset{\text{discharge}}{\rightleftharpoons}} [FeCl_4]^{2-} \tag{4.4}$$

The performance reported for all-iron RFBs is poor, with an energy efficiency of only 50%. This is attributed to the combination of parasitic losses due to hydrogen evolution and poor deposition/stripping kinetics at the negative electrode [71, 72]. The development of an all-iron RFB exhibiting appreciable energy efficiency is a subject worthy of considerable effort due to the exceptional abundance of iron, environmental compatibility and the ability to undergo two redox reactions separated by a non-trivial difference in potential.

As the kinetics of the iron deposition reaction were found to also hinder the energy efficiency of the RFB presented in this thesis, the zinc deposition and stripping reaction, shown in reaction 4.5, was also tested as an alternative. Due to its facile kinetics this reaction is widely utilized as the negative electrode reaction by both the academic and commercial RFB communities [73, 74].

$$\text{Negative electrode: } [\mathrm{ZnCl_4}]^{2-} + 2\,\mathrm{e}^- \underset{\text{discharge}}{\overset{\text{charge}}{\rightleftharpoons}} \mathrm{Zn} + 4\,\mathrm{Cl}^- \tag{4.5}$$

Global electricity production is currently around $2 \cdot 10^{16}$ W h/y. A modest goal of building sufficient RFB capacity to balance only 5% of this load using either Zn, Cu or Fe would require 4, 9, or 0.08 % respectively of global production capacity, if commissioned over a ten year period. Application of any transition metal, other than iron, in a typical RFB to achieve substantial balancing of global electricity production would likely either require slow implementation over many decades or a large increase in current production levels, which is a difficult undertaking.

The production of materials used in the preparation of DES is even more problematic, requiring a mega-tonne (MT) scale for the modest example considered here. US ethylene glycol production is around the 4 MT/y scale and global production has increased rapidly at sites with abundant natural gas deposits [75]. The production of quaternary ammonium salts is far more modest, with 100 kT/y being typical for a commonly used salt, such as choline chloride [76]. This indicates that the scale of the problem will most likely require the use of aqueous media or simple molten salt systems.

The discussion in the preceeding few paragraphs is only intended to demonstrate that the scale of electricity production is substantial and therefore efforts to support a large-scale transition to renewable energy using electrochemical systems are likely to founder unless they are based on realistic assumptions regarding the availability of the necessary materials [16]. While a certain amount of leeway is allowable regarding the timing or the scale of such a transition, or increases in future production levels, it is important that claims that any particular RFB technology can play a meaningful role are validated. Otherwise, resources could be wasted developing obsolete technologies.

This is clearly an invitation for electrochemists to explore the effect of experimental parameters, such as solvent, ligand chemistry and temperature, for a range of plausible transition metals.

4.3 Experimental RFB system

For initial studies the use of permeability cells was found to be ideal. The structure of a permcell based redox flow battery is shown in figure 4.2. This cell design minimizes the ingress of oxygen, which will oxidize the reduced species. It also facilitates precise temperature control and reduces both the size of the electrodes and the amount of electrolyte required. Importantly, since the material of construction of the two half-cells is glass, continual observation of the state of the electrode surface is possible. Integration of the electrolyte storage and convection in to the same space as the electrodes results in an extremely simple design.

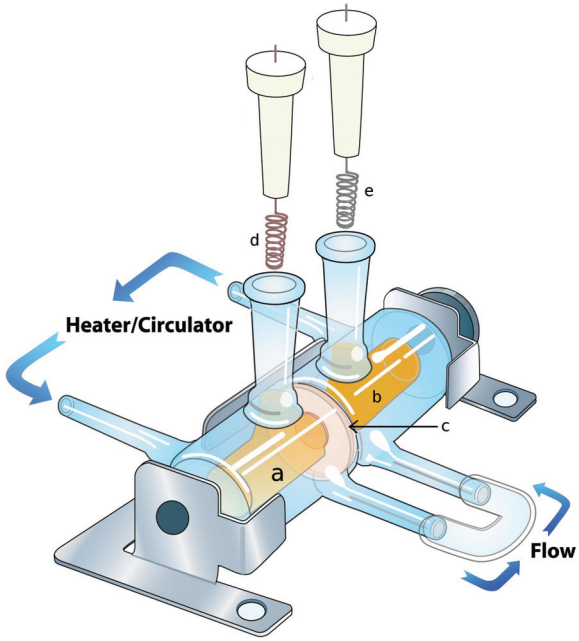

Figure 4.2. Illustration of the redox battery system utilised in this thesis. a and b are the two half-cells, c is the composite separator which prevents mixing of the electrolytes in the two half-cells. d and e are the two electrodes, which pass through a polypropylene stopper to ensure tight sealing. Convection is maintained by a pair of magnetic stirrers rotating in close proximity to the electrodes

Significant work was originally undertaken to develop larger RFB cells

with the common 'sandwich' configuration. Unfortunately, the temperature of the electrolytes would drop between the thermostatted reservoirs and the cells and as a result precipitation of the salts from the electrolyte was observed. A related problem was the slow and uneven pumping characteristics of the peristaltic pumps used, this resulted in poor convection, extremely low current densities and blockages due to precipitation. However the biggest problem observed was the ingress of oxygen, which in the case of Cu(I) electrolytes resulted in the formation of a green Cu(I) complex.

4.4 Novel separators for IL based RFBs

The application of commercially available separator materials in RFBs based on DES was not successful, as a rapid decrease in conductivity is observed on contact with the DES. This may be due to dehydration of the membrane due to the hygroscopic nature of DES. In this thesis the development of jellified deep eutectic solvents as a means to prepare separators for RFBs was performed. Jellification of ionic liquids using a polymer to form a rubbery solid electrolyte is common practice, for instance Angell jellified a range of lithium salts using polypropylene oxide [77]. More recently, Abbot developed a biodegradable composite with good mechanical properties based on a mixture of a DES and starch [78].

A jellified DES was prepared by adding 5wt.% polyvinyl alcohol (PVA, Mowiol 4-98, Mw 27,000) to plain ethaline. The suspension of PVA flakes was heated in a covered beaker to 150 °C on a hotplate with stirring. After 90 minutes all the PVA dissolved to form a clear, colourless liquid. Upon cooling, a translucent gel is formed, which can be returned to the liquid state an indefinite number of times by reheating briefly to 150 °C. The gel formed is sufficiently solid to prevent any convective flow, however it lacks sufficient mechanical strength to be used as a thin film separator in a RFB. For this reason, composite separators were prepared by applying the hot suspension sequentially to both sides of a vertically suspended filter paper (Schleicher & Schuell, 589/1) and removing any excess using a flat spatula.

The conductivity of jellified ethaline was determined by EIS measurements of a gel that had been cast in a PTFE cylinder, of known geometry,

which was sandwiched between two thermostated aluminium electrodes. The conductivity of the composite separator was determined in a similar manner, by sandwiching a sample between two copper discs inside the PTFE cylinder.

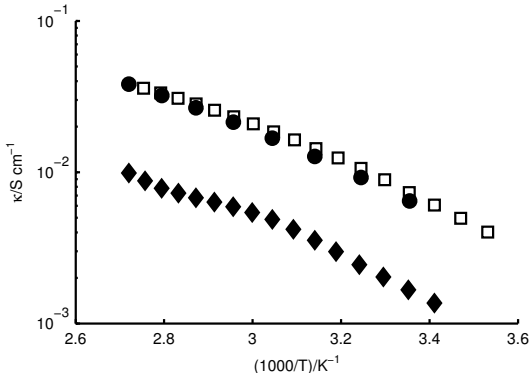

Figure 4.3. Temperature dependence of conductivity for pure ethaline (❑), ethaline gel containing 5wt.% PVA (●) and ethaline gel supported in a filter paper (◆). Publication III

Figure 4.3 shows that the plain and jellified electrolyte have virtually indistinguishable conductivity over a range of temperatures. The conductivity of the composite separator, also shown in figure 4.3, is around four times lower than the plain electrolyte or gel. As the thickness of the composite separator is 300 microns it should contribute only 30% of the ohmic losses in a typical sandwich configuration RFB. The conductivity of the gel prepared here is around three orders of magnitude higher than the DES-starch composite reported by Abbott [78].

4.5 EIS in RFBs

A problem with using perm cells is that the electrode separation is at least an order of magnitude larger than in a typical RFB. This means that the Ohmic losses in the cell will scale appreciably with current density, causing the switching conditions to be triggered prematurely at higher current densities. It is therefore necessary to quantify the Ohmic losses in the cell using EIS and compensate this to determine the effective cell potential. This decouples the investigation of basic cell chemistry and materials selection from optimization of the cell geometry.

When the value of R_s determined experimentally is compared with values predicted from ex-situ conductivity measurements they agree to within 20%. This shows that the process of decoupling works well and that it should be possible to perform accurate modeling of RFB performance by combining the knowledge gained from experiments that characterize the conductivity, viscosity and electrochemical reactivity of the system.

In principle, EIS measurements could be used rather effectively in an RFB to quantify more properties than just the Ohmic losses, because the cell geometry can be far more idealized than in a typical battery and the presence of convection should result in behaviour similar to that observed at a HDE, i.e. the attainment of a quasi steady-state in a matter of seconds and which can be maintained for extended periods if the electrolyte reservoirs are sufficiently large.

4.6 Steady-state voltammetry

A typical steady-state voltammogram for an all-copper RFB is shown in figure 4.4.

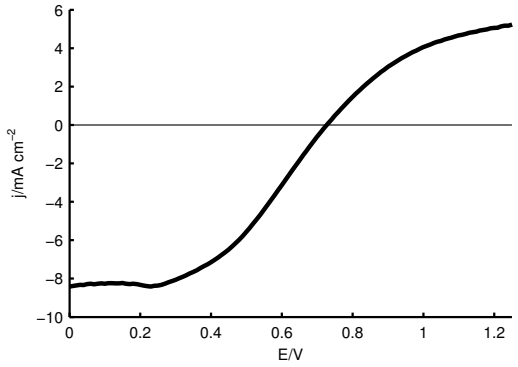

Figure 4.4. Staircase voltammogram of the all copper RFB. Publication III

Such a voltammogram allows the estimation of suitable charging or discharge currents, as well as appropriate switching potentials.

4.7 Charge cycling in IL based RFBs

Charge cycling is used to establish the long-term performance of batteries in an idealized and accelerated approximation of real world usage. It is

typically done by applying a constant current and switching at defined potentials. Integration of the current allows us to quantify the amount of charge passed during the charging and discharging stages, Q_{charge} and $Q_{\text{discharge}}$ respectively. The Coulombic efficiency, η_{Q}, for each cycle is then as defined in equation 4.6.

$$\eta_{\text{Q}} = \frac{Q_{\text{discharge}}}{Q_{\text{charge}}} \tag{4.6}$$

Also we can define the discharge capacity, which is the amount of charge withdrawn from the battery during any given cycle before the applicable switching potential condition is triggered, normalised by the theoretical capacity of the battery, Q_{theory}.

An important, but more problematic parameter to define when examining an RFB based on ILs is the energy efficiency of single charge-discharge cycle, η_{E}. The Ohmic losses are often significant in IL based systems and therefore the use of simple test systems which are not optimized to minimize these losses, such as the permeability cells used in this thesis, could lead to entirely incorrect conclusions regarding the energy efficiency achievable in a real system based on the same electrolytes. For this reason in this thesis the energy efficiency is calculated once the cell potential has been corrected for the Ohmic losses using equation 3.38 and then calculated using equation 4.7.

$$\eta_{\text{E}} = \frac{\sum_{t=t_{\text{switch}}}^{t=t_{\text{end}}} EI_{\text{discharge}} \Delta t}{\sum_{t=0}^{t=t_{\text{switch}}} EI_{\text{charge}} \Delta t} \tag{4.7}$$

A further refinement used in this thesis is to cancel the effect of variation in η_{Q} on the energy efficiency when presenting data for a series of measurements. η_{Q} can, for instance, during the first few cycles be greater than 1 when going from a low to a high charging current as the system is initially 'overcharged' compared to the long term trend value. This leads to equally large oscillations in the observed energy efficiency for a single cycle, $\eta_{\text{E,obs}}$, and can be mistakenly interpreted as a genuinely high energy efficiency. This effect can be cancelled by applying equation 4.8, while still providing an entirely accurate representation of the energy efficiency for each cycle.

$$\eta_{\text{E}} = \eta_{\text{E,obs}} \frac{\overline{\eta_{\text{Q}}}}{\eta_{\text{Q}}} \tag{4.8}$$

4.8 Performance of an all-copper RFB

Figure 4.5 shows a typical CV for a $[CuCl_4]^{2-}$ containing electrolyte. The Cu(I)/Cu(II) reaction is located at positive potentials and is therefore the positive electrode reaction. At negative potentials the Cu^0/Cu(I) reaction takes place with relative ease. Figure 4.5 suggests a cell potential of around 1V and this is found in practise too.

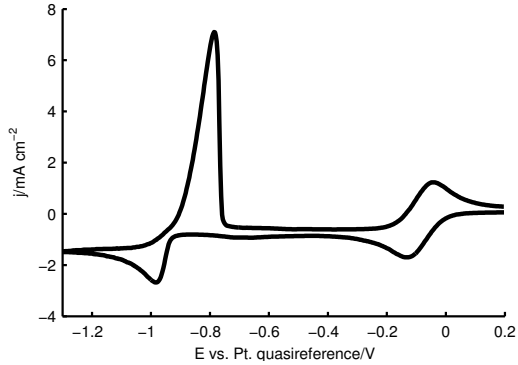

Figure 4.5. Cyclic voltammogram showing reactions 4.1 and 4.2 at a GC RDE. The electrolyte was a 20 mM solution of $CuCl_2$ in ethaline at 50 °C. The CV was initiated from a potential of 0.2 V. Publication III

A RFB that uses these reactions shows reasonable performance over many cycles and shows only minor deterioration within the period the cell was tested, as shown in figure 4.6. When the current used for charging and discharging is adjusted η_Q fluctuates strongly for the next few cycles. The discharge capacity of the system shows a particularly strong dependency on variations in the current used, with higher currents resulting in poor discharge capacities.

Cycling was performed at a current density of 10 mA/cm^2, with the exception of cycles 8 to 9 and 24 to 27 which were performed at current densities of 4 and 7.5 mA/cm^2 respectively. The pronounced outliers in η_Q correlate with changes in the applied current density and resolve within a few cycles.

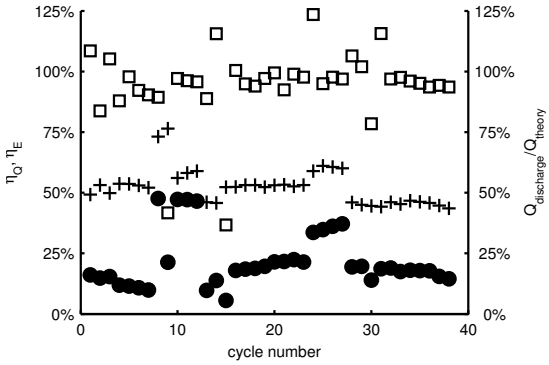

Figure 4.6. The evolution of Coulombic efficiency, η_Q (❑), energy efficiency, η_E (✚), and the discharge capacity, $Q_{\text{discharge}}$(●), normalised by the theoretical capacity, Q_{theory}. Publication III

4.9 Performance of an all-iron RFB

Figure 4.7 shows the deposition and stripping of iron from an ethaline based electrolyte containing the $[FeCl_4]^-$ complex. Nucleation of iron on GC is slow. Even once nucleation has taken place, there is still no mass tranport limited plateau in the deposition process prior to the onset of electrolyte decomposition. The stripping of iron is also not facile. The decomposition reaction appears to be favoured by an iron surface, which is not the case for copper.

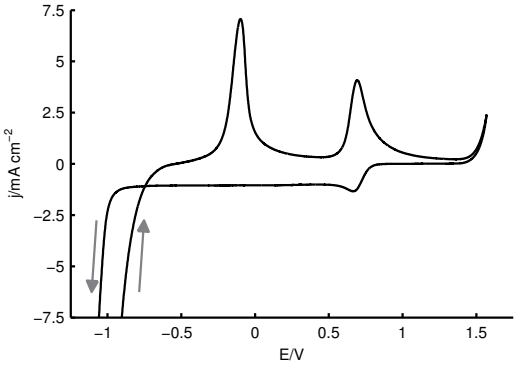

Figure 4.7. Cyclic voltammogram showing reactions 4.3 and 4.4 at a GC RDE. The electrolyte was a 20 mM solution of $FeCl_3$ in ethaline at 50 °C. The arrows indicate the start and end of the voltammogram. Publication IV

Figure 4.8 shows a Tafel plot representation of the data in figure 4.7 measured during the initial stripping process, which is observed immediately after the sweep initiates. Based on this the heterogeneous rate

constant, k^0 of the deposition reaction is estimated to be $2.1 \cdot 10^{-4}$ cm/s at 50 °C. This is around 15 times lower than k^0 for the Fe(II)/Fe(III) reaction under similar conditions.

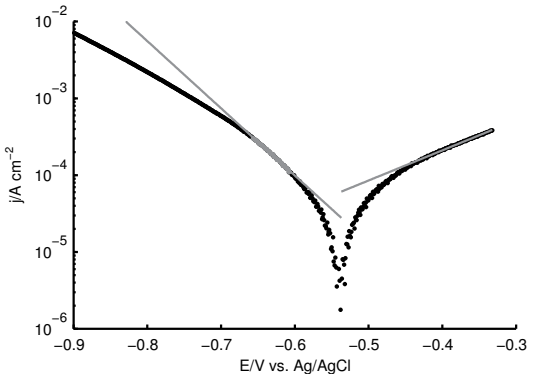

Figure 4.8. Tafel plot representation of the initial part of voltammogram shown in figure 4.7. The experimental data used to determine j_0 is highlighted. Publication IV

When these reactions are applied in an RFB the cell potential varies between 0.75 and 1.25V for the discharged and charged states respectively. Most problematic is that decomposition of the electrolyte in the perm. cell based system leads to the electrolyte being forced out of the cell, which slowly results in a loss of discharge capacity. The slow kinetics of the deposition reaction results in poor values of η_E, typically 35 to 40 %, irrespective of the current density used.

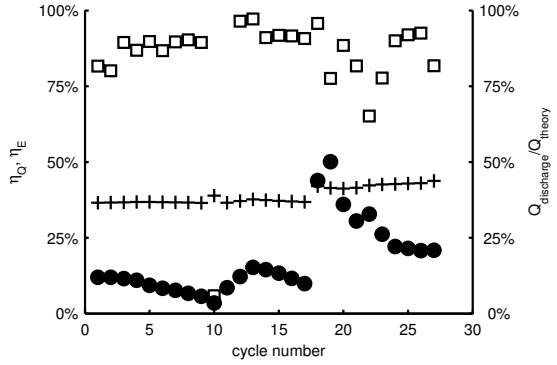

Figure 4.9. Evolution of Coulombic efficiency, η_Q (❑), energy efficiency, η_E (✚), and the discharge capacity, $Q_{discharge}$(●), normalised by the theoretical capacity, Q_{theory}, for the all-iron redox battery. Publication IV

4.10 Performance of a zinc-iron RFB

A steady-state voltammogram for an electrolyte prepared by reducing $[FeCl_4]^-$ using metallic zinc is shown in figure 4.10. This demonstrates the facile deposition and stripping of a metallic deposit. This is separated from two anodic processes by around 1V, which would predict a similar cell potential to that observed for the all-copper and all-iron batteries already discussed. The presence of two anodic process, combined with the unusually high stability of the Zn(II)-Fe(II) electrolyte against oxidation by oxygen suggests the formation of a Zn-Fe complex in solution.

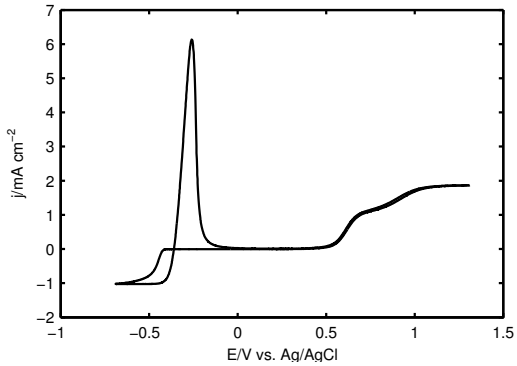

Figure 4.10. Cyclic voltammogram showing the facile deposition and stripping reaction and two oxidation processes for a Zn-Fe system at a GC RDE. The electrolyte was a 20 mM solution of $FeCl_3$ in ethaline that had been fully reacted with metallic zinc. Publication IV

Well formed plateau currents are observable at both ends of the window, which compares favourably to the results for the all-iron system shown in figure 4.7.

Figure 4.11 shows the steady performance and reasonable energy efficiency attained using the same electrolyte in a Zn-Fe battery over 25 cycles. η_E is significantly higher than that observed for the all-iron system. This is almost certainly due to the facile kinetics of metal deposition and stripping.

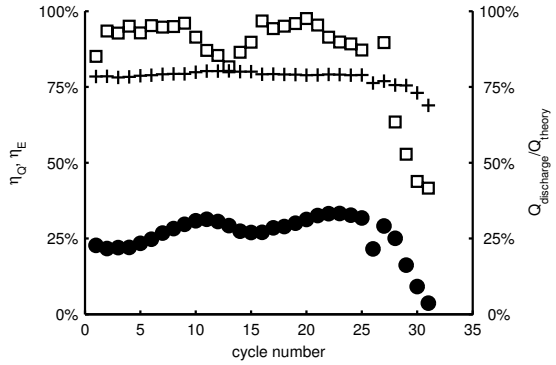

Figure 4.11. Evolution of Coulombic efficiency, η_Q (❑), energy efficiency, η_E (✚), and the discharge capacity, $Q_{discharge}$(●), normalised by the theoretical capacity, Q_{theory}, for the Zn-Fe redox battery. Publication IV

It was only during the writing of this thesis that it became clear to the author that the so-called 'zinc-air' RFB technology currently undergoing commercialisation by ViZn energy systems is in fact based on similar redox reactions to those reported here and therefore these are actually Zn-Fe batteries.

5. Conclusions and recommendations

5.1 Electrochemical techniques

The use of EIS is almost unavoidable if quantitative electrochemical measurements are to be performed in a DES or IL. This thesis has presented a range of techniques, based around EIS, to fully characterise the key parameters of electrochemical processes and systems. In particular, when EIS is combined with steady-state voltammetry at a HDE, a simple and accurate analysis is possible. This approach is likely to be equally applicable in other solvents and this should be validated.

It has been clearly shown that for quantitative techniques based on EIS to work well in any medium the reference electrode needs to possess a suitably low impedance. This is an area where DES and ILs can be expected to struggle more than other solvents, due to their relatively poor conductivity, and is a matter which is clearly not discussed sufficiently in the literature. This may explain why techniques, such as EIS or high speed voltammetry, have not been more commonly applied. The simplest method to overcome these limitations appears to be the twin reference electrode system reported in this thesis.

The application of the WTE as a tool to characterise the properties of an electrochemical reaction has been shown to work, especially when combined with EIS measurements. To be competitive with the RDE, the WTE system described in this thesis needs to be scaled down by a at least one order of magnitude to use a similar volume of electrolyte as the RDE and allow equally facile control of temperature.

The use of a WTE, or a similar flow cell, as the basis for determining the relative abundance of the oxidised and reduced species in electrolytes used in RFBs appears possible. Since the electrolyte is already being pumped only a WTE cell, inert QRE and simple potentiostat needs to be implemented. Importantly, this does not rely on potentiometric measurements between two eletrolytes, which can be sensitive to surface contamination of the sense electrodes. More importantly, this technique would provide absolute compositions for each electrolyte independently. This can be useful in quantifying the effects of parasitic reactions, such as hydrogen evolution, which may only occur at one electrode and lead to imbalance in the state-of-charge on each side. Since the objective is to quantify limiting currents, a simple QRE is more than sufficient.

5.2 Electrochemical applications of DES

It is striking that the complexes formed in DES tend to be uniformly similar to those formed in a range of chloride-rich solvents, even including concentrated HCl solutions. This appears to validate the minority view that molten metal hydrates may, in some cases, show more similarity to ionic liquids than aqueous solutions from the perspective of electrochemical applications. It also shows that the results from studies performed in chloride-rich chloroaluminates are often directly equivalent to the behaviour which will be observed in DES. So while it may be possible that over a million different ILs can be synthesised, this does not mean that the electrochemistry for each will be unique. In the case of transition metal electrochemistry, it is the metal complex formed that appears to almost entirely determine the behaviour of the system.

For this reason it is particularly desirable to have reliable, simple methods to determine the structure of the complex formed. The common practise is to compare UV-VIS measurements with results from earlier measurements that typically combine UV-VIS measurements and potentiometric titration. This places a heavy burden on the reliability of the earlier work and, in the case of potentiometric titration, assumes complexes possessing only a single type of ligand, which is a questionable assumption. Clearly, greater use of techniques such as Raman and NMR spectroscopy can allow these old structure assignments to be validated and

allow a better understanding of the fundamental nature of the materials being studied.

Ultimately, there appears to be little benefit to be gained from the use of DES as media for electrochemical processes. In their current form they lack the potential for outstandingly large potential windows that many regular ILs exhibit, while simultaneously being significantly more expensive, viscous and resistive than aqueous systems. While ILs overcome the narrow window of electrochemical stability they only do this at even greater expense and have equally poor transport properties. The use of elevated temperatures mitigates this problem somewhat, but brings the IL community back full circle to it's original starting point, namely molten salts. Since these are well known and have already found a small number of niche applications (such as the Hall-Héroult process to produce aluminium) it would appear to the author that much of the enthusiasm for DES and ILs in electrochemical applications is misplaced.

5.3 Redox Flow Batteries based on copper, iron or zinc

An all-copper RFB has been shown to work in a DES, with a particularly high Coulombic efficiency. However, the low current densities, high Ohmic losses and added cost of the DES make any practical system unlikely. An aqueous system based on chlorocomplexes, which would be analogous to the all-iron battery studied by Hruska and Savinell [71], is however certainly worthy of study. Relatively low cell potentials would require high solubility of the copper complexes to achieve energy and power densities comparable to state-of-the-art RFB technology. Other complexes may also increase the cell potential to more useful levels.

The all-iron RFB reported in this thesis shows similar problems to the aqueous systems reported by other authors. This suggests that the key issue is the complex formed and benefit may be found gained from a switch to a chloride free system using other ligands. Temperature is also a parameter of interest as the electrodeposition of iron appears to benefit from elevated temperature and the cell potential also appears to rise. In this one respect ILs and DES can serve as a useful platform to test the electrochemistry of transition complexes at elevated temperatures, without the added complexity of solvent evaporation or complexation by water.

The chloride based zinc-iron RFB presented here does not appear to have been reported in the literature. Since acid chloride baths for the electroplating of zinc are widely used and the electrochemistry of aqueous Fe(II)/Fe(III) chlorocomplexes is well know it is plausible that an aqueous zinc-iron chloride RFB could be developed. This concept is worthy of examination since zinc and iron are both abundant and relatively benign transition metals and the two metals appear to form an unusual dimetallic chloro complex.

The main hope for successful application of DES in RFB applications is that the high temperature transport properties of chlorometallate systems, such as the chloroferrates and chlorozincates reported by Abbott and others, are good. However, this is semantic trickery, since these are clearly ILs and have only been successfully co-opted by the DES community due to their low status compared to chloroaluminates. Irrespective of pointless terminological disputes, the separator remains a major problem for such systems since the polymeric materials typically used in RFBs tend to not work at higher temperatures or fail to function in non-aqueous media.

The benefit of using test cells optimised for exploratory work on novel liquids and redox chemistries has been shown in this thesis. The permeability cells used were in no way optimised for the application and better designed cells could certainly improve convection and reduce Ohmic losses, without necessarily reducing operational simplicity or increasing the minimal electrolyte volumes needed. It has been shown in this thesis that the Ohmic losses in an RFB can be accurately corrected by performing EIS measurements, this eliminates a major design constraint in experimental test systems (namely that the two electrodes are in close proximity) and could even allows the use a simple salt bridge.

Bibliography

[1] D. R. MacFarlane, S. A. Forsyth, J. Golding, and G. B. Deacon, "Ionic liquids based on imidazolium, ammonium and pyrrolidinium salts of the dicyanamide anion," *Green Chem.*, vol. 4, pp. 444–448, 2002.

[2] G. B. Appetecchi, S. Scaccia, C. Tizzani, F. Alessandrini, and S. Passerini, "Synthesis of hydrophobic ionic liquids for electrochemical applications," *Journal of The Electrochemical Society*, vol. 153, no. 9, pp. A1685–A1691, 2006.

[3] J. Fuller, R. T. Carlin, and R. A. Osteryoung, "The room temperature ionic liquid 1-ethyl-3-methylimidazolium tetrafluoroborate: Electrochemical couples and physical properties," *Journal of The Electrochemical Society*, vol. 144, no. 11, pp. 3881–3886, 1997.

[4] A. P. Abbott, R. C. Harris, and K. S. Ryder, "Application of hole theory to define ionic liquids by their transport properties," *The Journal of Physical Chemistry B*, vol. 111, no. 18, p. 4910, 2007.

[5] T. M. Laher and C. L. Hussey, "Copper(I) and copper(II) chloro complexes in the basic aluminum chloride-1-methyl-3-ethylimidazolium chloride ionic liquid," *Inorganic Chemistry*, vol. 22, no. 22, pp. 3247–3251, 1983.

[6] C. Nanjundiah and R. A. Osteryoung, "Electrochemical Studies of Cu(I) and Cu(II) in an Aluminum Chloride-N-(n-Butyl)Pyridinium Chloride Ionic Liquid," *Journal of The Electrochemical Society*, vol. 130, no. 6, pp. 1312–1318, 1983.

[7] A. A. Fannin, D. A. Floreani, L. A. King, J. S. Landers, B. J. Piersma, D. J. Stech, R. L. Vaughn, J. S. Wilkes, and W. J. L., "Properties of 1,3-dialkylimidazolium chloride-aluminum chloride ionic liquids. 2. phase transitions, densities, electrical conductivities, and viscosities," *The Journal of Physical Chemistry*, vol. 88, no. 12, pp. 2614–2621, 1984.

[8] S. Z. E. Abedin and F. Endres, "Ionic liquids: The link to high-temperature molten salts?," *Accounts of Chemical Research*, vol. 40, no. 11, pp. 1106–1113, 2007.

[9] A. P. Abbott and K. J. McKenzie, "Application of ionic liquids to the electrodeposition of metals," *Phys. Chem. Chem. Phys.*, vol. 8, p. 4265, 2006.

[10] C. A. Angell, *Ionic Liquids in the Temperature Range 150-1500 K: Patterns and Problems, in Molten Salts and Ionic Liquids: Never the Twain? (eds. M. Gaune-Escard and K. Seddon)*. John Wiley and Sons, Inc., 2010.

[11] M. Schlesinger and M. Paunovic, *Modern Electroplating*. John Wiley & Sons, Inc., 2010.

[12] F. H. Hurley and T. P. Wier, "The electrodeposition of aluminum from nonaqueous solutions at room temperature," *Journal of The Electrochemical Society*, vol. 98, no. 5, pp. 207–212, 1951.

[13] K. Ziegler and H. Lehmkuhl, "Die elektrolytische abscheidung von aluminium aus organischen komplexverbindungen," *Zeitschrift für anorganische und allgemeine Chemie*, vol. 283, no. 1-6, pp. 414–424, 1956.

[14] C.-H. Dustmann, "Advances in zebra batteries," *Journal of Power Sources*, vol. 127, no. 1–2, pp. 85 – 92, 2004.

[15] M. Skyllas-Kazacos, M. H. Chakrabarti, S. A. Hajimolana, F. S. Mjalli, and M. Saleem, "Progress in flow battery research and development," *Journal of The Electrochemical Society*, vol. 158, no. 8, p. R55, 2011.

[16] C. Wadia, P. Albertus, and V. Srinivasan, "Resource constraints on the battery energy storage potential for grid and transportation applications," *Journal of Power Sources*, vol. 196, no. 3, p. 1593, 2011.

[17] N. V. Plechkova and K. R. Seddon, "Applications of ionic liquids in the chemical industry," *Chem. Soc. Rev.*, vol. 37, pp. 123–150, 2008.

[18] P. Walden, "Ueber die molekulargrösse und elektrische leitfähigkeit einiger geschmolzenen salze," *Bull. Acad. Imper. Sci. St. Petersbourg*, vol. 8, pp. 405–422, 1914.

[19] T. Tsuda and C. L. Hussey, *Electrochemistry of Room-Temperature Ionic Liquids and Melts*, vol. 45 of *Modern Aspects of Electrochemistry*. Springer, New York, 2009.

[20] J. S. Wilkes, J. A. Levisky, R. A. Wilson, and C. L. Hussey, "Dialkylimidazolium chloroaluminate melts: a new class of room-temperature ionic liquids for electrochemistry, spectroscopy and synthesis," *Inorganic Chemistry*, vol. 21, no. 3, pp. 1263–1264, 1982.

[21] X. Sun, Y. Ji, L. Guo, J. Chen, and D. Li, "A novel ammonium ionic liquid based extraction strategy for separating scandium from yttrium and lanthanides," *Separation and Purification Technology*, vol. 81, no. 1, pp. 25 – 30, 2011.

[22] C. M. Starks, "Phase-transfer catalysis. i. heterogeneous reactions involving anion transfer by quaternary ammonium and phosphonium salts," *Journal of the American Chemical Society*, vol. 93, no. 1, pp. 195–199, 1971.

[23] A. M. O'Mahony, D. S. Silvester, L. Aldous, C. Hardacre, and R. G. Compton, "Effect of water on the electrochemical window and potential limits of roomtemperature ionic liquids," *Journal of Chemical Engineering Data*, vol. 53, no. 12, pp. 2884–2891, 2008.

[24] T. P. T. Pham, C.-W. Cho, and Y.-S. Yun, "Environmental fate and toxicity of ionic liquids: A review," *Water Research*, vol. 44, no. 2, pp. 352 – 372, 2010.

[25] A. Heintz and C. Wertz, "Ionic liquids: A most promising research field in solution chemistry and thermodynamics," *Pure and Applied Chemistry*, vol. 78, no. 8, pp. 1587–1593, 2006.

[26] R. Al-Salman, S. Z. El Abedin, and F. Endres, "Electrodeposition of Ge, Si and SiGe from an air and water-stable ionic liquid," *Phys. Chem. Chem. Phys.*, vol. 10, pp. 4650–4657, 2008.

[27] D. Cunningham, M. Rubcich, and D. Skinner, "Cadmium telluride pv module manufacturing at bp solar," *Progress in Photovoltaics: Research and Applications*, vol. 10, no. 2, pp. 159–168, 2002.

[28] A. P. Abbott, G. Capper, D. L. Davies, R. K. Rasheed, and V. Tambyrajah, "Novel solvent properties of choline chloride/urea mixtures," *Chem. Commun.*, p. 70, 2003.

[29] A. P. Abbott, D. Boothby, G. Capper, D. L. Davies, and R. K. Rasheed, "Deep eutectic solvents formed between choline chloride and carboxylic acids : versatile alternatives to ionic liquids," *Journal of the American Chemical Society*, vol. 126, no. 29, p. 9142, 2004.

[30] A. P. Abbott, G. Capper, K. J. McKenzie, A. Glidle, and K. S. Ryder, "Electropolishing of stainless steels in a choline chloride based ionic liquid: an electrochemical study with surface characterisation using sem and atomic force microscopy," *Phys. Chem. Chem. Phys.*, vol. 8, p. 4214, 2006.

[31] A. P. Abbott, K. El Ttaib, G. Frisch, K. J. McKenzie, and K. S. Ryder, "Electrodeposition of copper composites from deep eutectic solvents based on choline chloride," *Phys. Chem. Chem. Phys.*, vol. 11, p. 4269, 2009.

[32] K. Haerens, E. Matthijs, K. Binnemans, and B. Van der Bruggen, "Electrochemical decomposition of choline chloride based ionic liquid analogues," *Green Chem.*, vol. 11, p. 1357, 2009.

[33] A. Abbott, J. Barron, K. Ryder, and D. Wilson, "Eutectic-based ionic liquids with metal-containing anions and cations," *Chemistry – A European Journal*, vol. 13, no. 22, pp. 6495–6501, 2007.

[34] J. Estager, P. Nockemann, K. R. Seddon, M. Swadzba-Kwasny, and S. Tyrrell, "Validation of Speciation Techniques: A Study of Chlorozincate(II) Ionic Liquids," *Inorganic Chemistry*, vol. 50, no. 11, p. 5258, 2011.

[35] T. Vainikka, "Electrodeposition of metals from ionic liquids," MSc thesis, Helsinki University of Technology, 2008.

[36] T. Vainikka, D. Lloyd, L. Murtomäki, J. A. Manzanares, and K. Kontturi, "Electrochemical study of copper chloride complexes in the RTIL 1-butyl-1-methylpyrrolidinium bis(trifluoromethylsulfonyl)imide," *Electrochimica Acta*, vol. 87, no. 0, p. 739, 2013.

[37] A. P. Abbott, K. El Ttaib, K. S. Ryder, and E. L. Smith, "Electrodeposition of nickel using eutectic based ionic liquids," *Transactions of the Institute of Metal Finishing*, vol. 86, no. 4, pp. 234–240, 2008.

[38] A. P. Abbott, J. C. Barron, G. Frisch, K. S. Ryder, and A. F. Silva, "The effect of additives on zinc electrodeposition from deep eutectic solvents," *Electrochimica Acta*, vol. 56, no. 14, p. 5272, 2011.

[39] R. Böck and S. Wulf, "Electrodeposition of iron films from an ionic liquid (ChCl/urea/$FeCl_3$ deep eutectic mixtures)," *Transactions of the Institute of Metal Finishing*, vol. 87, no. 1, p. 28, 2009.

[40] A. P. Abbott, G. Capper, D. L. Davies, and R. K. Rasheed, "Ionic liquid analogues formed from hydrated metal salts," *Chemistry – A European Journal*, vol. 10, no. 15, pp. 3769–3774, 2004.

[41] T. Scheffler and M. Thomson, "Novel ambient temperature ionic liquids formulated from 1-methyl-3-ethylimidazolium chloride and anhydrous metal chloride," *Proc. Electrochem. Soc.*, vol. 10, pp. 281–289, 1990.

[42] C. Amuli, M. Elleb, J. Meullemeestre, M. J. Schwing, and F. Vierling

[43] S. Mishra and N. Devi, "Extraction of copper(II) from hydrochloric acid solution by Cyanex 921," *Hydrometallurgy*, vol. 107, no. 1–2, pp. 29 – 33, 2011.

[44] S. A. Bolkan and J. T. Yoke, "Room Temperature Fused Salts Based on Copper(I) Chloride-1-Methyl-3-Ethylimidazolium Chloride Mixtures: III . Electrochemical Studies," *Journal of The Electrochemical Society*, vol. 134, no. 7, pp. 1698–1702, 1987.

[45] M. S. Sitze, E. R. Schreiter, E. V. Patterson, and R. G. Freeman, "Ionic Liquids Based on $FeCl_3$ and $FeCl_2$. Raman Scattering and ab Initio Calculations," *Inorganic Chemistry*, vol. 40, no. 10, p. 2298, 2001.

[46] W. Xu, E. I. Cooper, and C. A. Angell, "Ionic liquids: ion mobilities, glass temperatures, and fragilities," *The Journal of Physical Chemistry B*, vol. 107, no. 25, p. 6170, 2003.

[47] A. P. Abbott, G. Capper, D. L. Davies, and R. Rasheed, "Ionic liquids based upon metal halide/substituted quaternary ammonium salt mixtures," *Inorganic Chemistry*, vol. 43, no. 11, p. 3447, 2004.

[48] Y. Liu, G. Wu, and M. Qi, "Polymorphous crystals from chlorozincate-choline chloride ionic liquids in different molar ratios," *Journal of Crystal Growth*, vol. 281, no. 2–4, p. 616, 2005.

[49] R. S. Nicholson, "Theory and application of cyclic voltammetry for measurement of electrode reaction kinetics.," *Analytical Chemistry*, vol. 37, no. 11, pp. 1351–1355, 1965.

[50] J. O'Dea, J. Osteryoung, and T. Lane, "Determining kinetic parameters from pulse voltammetric data," *The Journal of Physical Chemistry*, vol. 90, no. 12, pp. 2761–2764, 1986.

[51] T. Vainikka, "Private communication," 2013.

[52] C. Gabrielli, *Identification of electrochemical processes by frequency response analysis, Issue 3*. Solartron Analytical, 1998.

[53] M. Lourakis, "Levmar : Levenberg–Marquardt Nonlinear Least Squares Algorithms in C/C++," March 2011.

[54] G. Snook, A. Best, A. Pandolfo, and A. Hollenkamp, "Evaluation of a Ag/Ag^+ reference electrode for use in room temperature ionic liquids," *Electrochemistry Communications*, vol. 8, no. 9, p. 1405, 2006.

[55] D. S. Silvester, E. I. Rogers, R. G. Compton, K. J. McKenzie, K. S. Ryder, F. Endres, D. MacFarlane, and A. P. Abbott, *Technical Aspects, in Electrodeposition from Ionic Liquids (eds F. Endres, D. MacFarlane and A. Abbott)*, p. 287. Wiley-VCH Verlag GmbH, 2008.

[56] Gamry Instruments Inc., *Technical note: Measuring the Impedance of Your Reference Electrode*, 2010.

[57] Princeton Applied Research, *Technical note: Potentiostat Stability Considerations*, 2010.

[58] Corning Incorporated, *Datasheet: VYCOR Brand Porous Glass 7930*, 2001.

[59] M. Lipsztajn and R. A. Osteryoung, "Electrochemistry in neutral ambient-temperature ionic liquids. 1. Studies of iron(III), neodymium(III), and lithium(I)," *Inorganic Chemistry*, vol. 24, no. 5, p. 716, 1985.

[60] S. Treimer, A. Tang, and D. Johnson, "A Consideration of the Application of Koutecký-Levich Plots in the Diagnoses of Charge-Transfer Mechanisms at Rotated Disk Electrodes," *Electroanalysis*, vol. 14, no. 3, pp. 165–171, 2002.

[61] J. A. Alden and R. G. Compton, "A data analysis service for steady-state voltammetry via the world wide web," *Electroanalysis*, vol. 10, no. 3, pp. 207–209, 1998.

[62] A. Bard and L. Faulkner, *Electrochemical Methods: Fundamentals and Applications*. Wiley, 2000.

[63] D. T. Chin and C. H. Tsang, "Mass transfer to an impinging jet electrode," *Journal of The Electrochemical Society*, vol. 125, no. 9, p. 1461, 1978.

[64] N. V. Rees, O. V. Klymenko, B. A. Coles, and R. G. Compton, "Hydrodynamics and Mass Transport in Wall-Tube and Microjet Electrodes: An Experimental Evaluation of Current Theory," *The Journal of Physical Chemistry B*, vol. 107, no. 49, p. 13649, 2003.

[65] D. Lloyd, T. Vainikka, S. Schmachtel, L. Murtomäki, and K. Kontturi, "Simultaneous characterisation of electrode kinetics and electrolyte properties in ionic liquids using a rotating disc electrode," *Electrochimica Acta*, vol. 69, p. 139, 2012.

[66] W. J. Albery and S. Bruckenstein, "Uniformly accessible electrodes," *Journal of Electroanalytical Chemistry and Interfacial Electrochemistry*, vol. 144, no. 1, p. 105, 1983.

[67] H. Holttinen and coauthors, "Design and operation of power systems with large amounts of wind power, vtt research notes 2493," 2009.

[68] European Commision, "Renewable energy: Progressing towards the 2020 target," 2011.

[69] W. W. Porterfield and J. T. Yoke, *Inorganic Compounds with Unusual Properties*, ch. 10, pp. 104–111. ACS Publications, Washington D.C., 1976.

[70] B. Kratochvil and K. R. Betty, "A Secondary Battery Based on the Copper(II)/(I) and (I)/(0) Couples in Acetonitrile," *Journal of The Electrochemical Society*, vol. 121, no. 7, pp. 851–854, 1974.

[71] L. W. Hruska and R. F. Savinell, "Investigation of factors affecting performance of the iron redox battery," *J. Electrochem. Soc.*, vol. 128, no. 1, p. 18, 1981.

[72] A. K. Manohar, K. M. Kim, E. Plichta, M. Hendrickson, S. Rawlings, G. K. Surya Prakash, and S. R. Narayanan, "Studies on the iron-chloride redox flow battery for large-scale energy storage," in *Proceedings of the 223rd ECS Meeting*, 2013.

[73] G. Nikiforidis, L. Berlouis, D. Hall, and D. Hodgson, "Evaluation of carbon composite materials for the negative electrode in the zinc-cerium redox flow cell," *Journal of Power Sources*, vol. 206, no. 0, p. 497, 2012.

[74] A. Z. Weber, M. M. Mench, J. P. Meyers, P. N. Ross, J. T. Gostick, and Q. Liu, "Redox flow batteries: a review," *Journal of Applied Electrochemistry*, vol. 41, no. 10, p. 1137, 2011.

[75] M. W. Forkner, J. H. Robson, W. M. Snellings, A. E. Martin, F. H. Murphy, and T. E. Parsons, *Glycols, in Kirk-Othmer Encyclopedia of Chemical Technology*. John Wiley & Sons, Inc., 2000.

[76] C. E. Gidding, *Choline, in Kirk-Othmer Encyclopedia of Chemical Technology*. John Wiley & Sons, Inc., 2000.

[77] C. Angell, C. Liu, and E. Sanchez, "Rubbery solid electrolytes with dominant cationic transport and high ambient conductivity," *Nature*, pp. 137–139, 1993.

[78] A. P. Abbott, A. D. Ballantyne, J. P. Conde, K. S. Ryder, and W. R. Wise, "Salt modified starch: sustainable, recyclable plastics," *Green Chem.*, vol. 14, pp. 1302–1307, 2012.

Errata

Publication II

In equation 4 on page 140 the solute concentration should be in the numerator, not the denominator.

Publication III

In figure 5 on page 21 label on the ordinate axis should be $|I_k|/A$, not I_k/A.

Deep eutectic solvents are materials possessing similar properties to chloride rich ionic liquids. This enables them to readily dissolve a range of transition metal chloride salts to form chloro complexes. This thesis demonstrates the application of a range of analytical methods to characterize heterogeneous reactions involving these complexes, as well as methods to characterize the transport properties of the complexes and deep eutectic solvents. The application of these materials in redox flow batteries is also reported.

Aalto-DD 174/2013

ISBN 978-952-60-5403-2
ISBN 978-952-60-5404-9 (pdf)
ISSN-L 1799-4934
ISSN 1799-4934
ISSN 1799-4942 (pdf)

Aalto University
School of Chemical Technology
Depart of Chemistry
www.aalto.fi

BUSINESS + ECONOMY

ART + DESIGN + ARCHITECTURE

SCIENCE + TECHNOLOGY

CROSSOVER

DOCTORAL DISSERTATIONS